


# SPATC1L maintains the integrity of the sperm head-tail junction

Jihye Kim<sup>1</sup>, Jun Tae Kwon<sup>1</sup>, Juri Jeong<sup>1</sup>, Jaehwan Kim<sup>1</sup>, Seong Hyeon Hong<sup>1</sup>, Jinyoung Kim<sup>1</sup>, Zee Yong Park<sup>1</sup>, Kyung Hwun Chung<sup>1</sup>, Edward M Eddy<sup>2</sup> & Chunghee Cho<sup>1,\*</sup> 

## Abstract

Spermatogenesis is a tightly regulated process involving germ cell-specific and germ cell-predominant genes. Here we investigate a novel germ cell-specific gene, *Spatc1* (spermatogenesis and centriole associated 1 like). Expression analyses show that SPATC1L is expressed in mouse and human testes. We find that mouse SPATC1L localizes to the neck region in testicular sperm. Moreover, SPATC1L associates with the regulatory subunit of protein kinase A (PKA). Using CRISPR/Cas9-mediated genome engineering, we generate mice lacking SPATC1L. Disruption of *Spatc1* in mice leads to male sterility owing to separation of sperm heads from tails. The lack of SPATC1L is associated with a reduction in PKA activity in testicular sperm, and we identify capping protein muscle Z-line beta as a candidate target of phosphorylation by PKA in testis. Taken together, our results implicate the SPATC1L-PKA complex in maintaining the stability of the sperm head-tail junction, thereby revealing a new molecular basis for sperm head-tail integrity.

**Keywords** protein kinase A; SPATC1L; sperm; sperm head-tail; testis

**Subject Categories** Cell Adhesion, Polarity & Cytoskeleton; Development & Differentiation

**DOI** 10.15252/embr.201845991 | Received 21 February 2018 | Revised 25 June 2018 | Accepted 3 July 2018 | Published online 19 July 2018

**EMBO Reports (2018) 19: e45991**

## Introduction

Spermatogenesis, the process of male germ cell development, is a tightly regulated series of events that occur in successive mitotic, meiotic, and postmeiotic phases. During spermatogenesis, spermatogonial stem cells undergo mitotic proliferation, and primary spermatocytes undergo meiotic division to produce spermatids. Haploid round spermatids undergo dramatic morphological changes to become highly specialized sperm through events of cellular elongation and nuclear condensation, a process termed spermiogenesis [1,2]. The tight modulation of this developmental process suggests the expression of a highly organized network of genes. The regulation of gene expression during spermatogenesis occurs at three

levels: intrinsic, interactive, and extrinsic [3]. The intrinsic program in particular involves germ cell- and/or stage-specific genes, and determines which genes are utilized and when the genes are expressed. This tightly regulated process constitutes a unique feature of male reproduction and is important for successful male germ cell development.

Human infertility rates are currently high, and about half of such cases are caused by male infertility [4]. Understanding the molecular mechanisms underlying spermatogenesis is critical for diagnosing male infertility. Previous systematic *in silico* analyses of the round spermatid UniGene library (Lib.6786) and *in vitro* studies have identified a number of genes that are specifically expressed in the testis [5]. Further analyses predicted that these genes are involved in diverse functions during spermatogenesis and fertilization. One such recently identified gene is spermatogenesis and centriole associated 1 like (*Spatc1l*) (UniGene ID Mm.45611; GenBank accession number NM\_029661). The *Spatc1l* gene was named after a spermatogenesis and centriole associated 1 (*Spatc1*) gene which encodes a sperm centrosome protein showing partial amino acid sequence homology (~50%) with a protein encoded by *Spatc1l*. [6]. *Spatc1l* encompasses approximately an 8-kb region in mouse chromosome 10. The human ortholog of *Spatc1l* is located in a genomic region (chromosome 21q22.3) of conserved synteny between mice and humans. It was found that the mouse *Spatc1l* gene is transcribed exclusively in spermatogenic cells starting from day 20 after birth, when round spermatids appear in the seminiferous tubules in mice [5,7]. *Spatc1l* was predicted to encode a protein with 342 amino acids. A further study using an antibody against SPATC1L generated using a Glutathione-S-transferase (GST)-fusion protein showed that SPATC1L is specifically expressed as a 38-kDa protein in spermatogenic cells [8].

In this study, we investigated the characteristics and functions of SPATC1L protein during male germ cell development. Expression of SPATC1L started from spermatids and the protein was localized to the neck region in testicular sperm. A proteomic analysis revealed that SPATC1L interacts with the regulatory (R) subunit of cAMP-dependent protein kinase (PKA) in male germ cells, discovering a new PKA-binding protein. Using a *Spatc1l*-knockout (KO) mice generated by CRISPR/Cas9 genome editing, we found that male mice lacking *Spatc1l* were completely sterile owing to separation of

<sup>1</sup> School of Life Sciences, Gwangju Institute of Science and Technology, Gwangju, Korea

<sup>2</sup> Reproductive and Developmental Biology Laboratory, National Institute of Environmental Health Sciences, National Institutes of Health, Research Triangle Park, NC, USA  
\*Corresponding author. Tel: +82 62 715 2490; E-mail: choch@gist.ac.kr

sperm heads from sperm tails. We identified capping protein (actin filament) muscle Z-line beta (CAPZB) as a candidate protein regulated by the SPATC1L-PKA complex at the neck region of testicular sperm. Our various *in vitro* analyses showed that SPATC1L promotes PKA-mediated CAPZB phosphorylation and regulates the F-actin dynamics. Numerous cases of spermatozoa without heads (a.k.a. “acephalic”, “decapitated”, and “pin heads”) have been reported in infertile patients [9–16]. However, the molecular basis for the maintenance of sperm head-tail junction integrity has remained largely unknown. Our study provides new and comprehensive information about molecular mechanisms underlying stabilization of the sperm head-tail junction.

## Results

### SPATC1L is expressed in spermatogenic cells and is localized to the neck of testicular sperm

To characterize the SPATC1L protein, we first examined the developmental expression pattern of SPATC1L in germ cells during spermatogenesis. Immunoblot analyses, performed using an antibody against a GST fusion protein of a recombinant mouse SPATC1L fragment corresponding to amino acids 101–200 (Fig EV1A) [8], were performed on cells from different phases during sperm development, including testicular spermatogenic cells, testicular sperm, and mature sperm from the epididymis. The specificity of the antibody was verified by competitive immunoblotting analysis (Fig EV1B). The testicular spermatogenic cell population includes spermatogonia, spermatocytes, and round spermatids, whereas the testicular sperm population includes elongating and condensing spermatids, and fully developed sperm. The SPATC1L protein was expressed as a 38-kDa protein in testicular spermatogenic cells and testicular sperm, but was not detected in epididymal sperm, indicating developmentally regulated expression during spermatogenesis (Fig 1A). Because human SPATC1L shares 88% amino acid sequence homology with the mouse protein, we also examined the expression of SPATC1L in humans. Similarly, human SPATC1L was abundantly expressed in testes (Fig 1B). Further immunoblot analyses, carried out using mouse testis lysates obtained from different days after birth, showed that SPATC1L was first detected in the testis at day 20, corresponding to the beginning of the postmeiotic phase of spermatogenesis (Fig 1C).

To establish the cellular localization of SPATC1L, we performed immunofluorescence staining (Fig 1D). SPATC1L signals were first detected in round spermatids during spermatogenesis. In these cells, the protein appeared to be co-localized to the  $\gamma$ -tubulin staining-enriched region (centrosome). Subsequently during spermiogenesis, the SPATC1L signal was observed in regions separated from the  $\gamma$ -tubulin staining-enriched region presumed to be centrosome and finally was localized to the neck of testicular sperm in close proximity to the centriole. No SPATC1L signals were detected in mature sperm (Fig 1D), consistent with immunoblot data (Fig 1A). These results indicate that SPATC1L may function at the connecting piece of testicular sperm. To further investigate the subcellular localization of SPATC1L, we transiently transfected a Sertoli cell line (TM4 cells) with an expression construct for GFP-tagged mouse SPATC1L. We utilized TM4 cells because the cell line exhibited high

transfection efficiency in our various experiments. This analysis revealed a punctate or speckled localization pattern that partially overlapped with the centrosomal region (Fig EV1C). In contrast, upon transfection of cells with a deletion mutant of SPATC1L lacking the N-terminal coiled-coil domain, SPATC1L signals were detected in the nucleus and cytoplasm without the speckled pattern (Fig EV1D) suggesting that the coiled-coil domain is responsible for limited cellular occupation of SPATC1L.

### SPATC1L interacts with protein kinase A

To establish the functional characteristics of SPATC1L, we first identified SPATC1L-interacting proteins by immunoprecipitating protein lysates from mouse testis with an anti-SPATC1L antibody and subjecting precipitates to tryptic digestion, followed by mass spectrometry analysis. The anti-SPATC1L antibody effectively precipitated SPATC1L compared with control IgG (Fig 2A). Subsequent proteomic analyses identified SPATC1L-interacting proteins: protein kinase cAMP-dependent type I regulatory subunit alpha (PRKAR1A, a.k.a. RI $\alpha$ ), protein kinase cAMP-activated catalytic subunit alpha isoform 2 (PRKACA isoform 2, a.k.a. C $\alpha$ 2), and A kinase anchor protein 11 (AKAP11) (Fig 2B). RI $\alpha$  and C $\alpha$ 2 are subunits of the cAMP-dependent PKA complex, which is composed of two R subunits and two catalytic (C) subunits. AKAP11 is a scaffolding protein that interacts with the R subunit of PKA [17,18]. To confirm these proteomic analysis results, we immunoprecipitated total lysates from mouse testes using an anti-SPATC1L antibody, and immunoblotted precipitates with anti-RI $\alpha$  and anti-C $\alpha$  antibodies. The anti-SPATC1L antibody effectively immunoprecipitated the cognate protein, and immunoblotting showed that the immunoprecipitated samples also contained RI $\alpha$  and C $\alpha$ 2 proteins, verifying the proteomic analysis data (Fig 2C). The proteomic analysis detected larger amount of RI $\alpha$  than C $\alpha$ 2 as a SPATC1L interacting protein, suggesting that SPATC1L primarily interacts with RI $\alpha$  and interacts indirectly with C $\alpha$ 2 through the SPATC1L-RI $\alpha$  complex in spermatogenic cells. Interaction between SPATC1L and RI $\alpha$  was also confirmed by reverse co-immunoprecipitation using an anti-RI $\alpha$  antibody (Fig EV2A).

As an initial step toward understanding the relationship between SPATC1L and PKA, we examined the expression pattern of the PKA subunits during spermatogenesis by performing immunoblot analyses on cells from different phases during sperm development. Whereas RI $\alpha$  and C $\alpha$ 2 were expressed in all cell types of spermatogenesis, C $\alpha$ 1 was expressed only in testicular spermatogenic cells (Fig 2D). To further investigate the expression pattern of PKA subunits in the testis, we performed immunoblot analysis using mouse testis lysates obtained at different days after birth. RI $\alpha$  was expressed in the testis at all mouse ages and C $\alpha$ 2 expression started on postnatal day 21, which corresponds to early part of the postmeiotic phase of spermatogenesis (Fig EV2B–D). This result is consistent with previous reports of transcriptional switching from the C $\alpha$ 1 isoform to the C $\alpha$ 2 isoform during spermatogenesis [19–21]. Notably, expression of C $\alpha$ 2 and SPATC1L proteins began at a similar stage during spermatogenesis.

To compare the cellular localization of SPATC1L and the major SPATC1L-interacting protein RI $\alpha$  during spermatogenesis, we performed a co-immunostaining analysis on spermatogenic cells. RI $\alpha$  was found to be distributed over a wide region of the cytoplasm

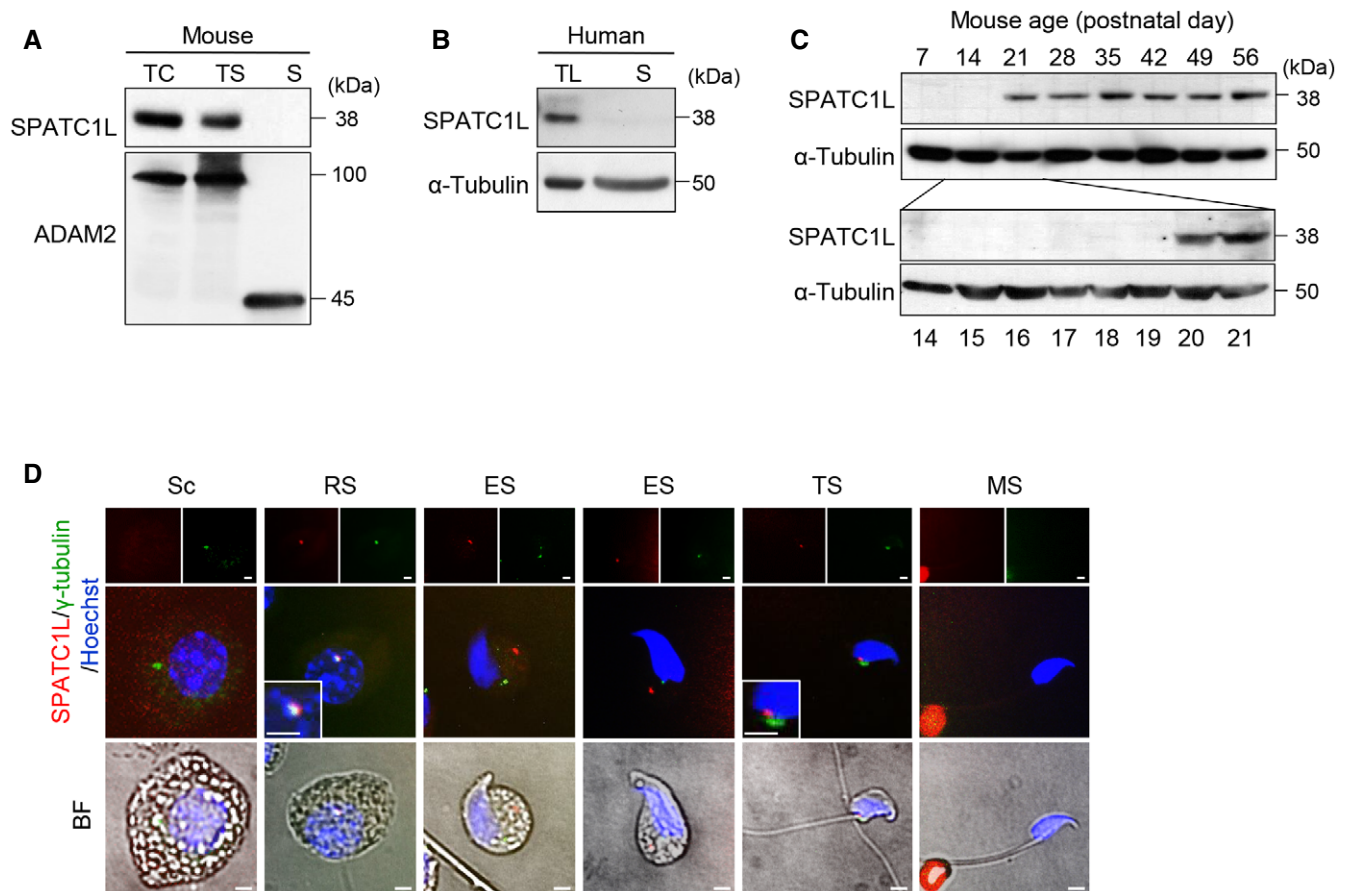


**Figure 1. Developmental expression and localization of SPATC1L.**

A Immunoblotting of SPATC1L in testicular cells (TC), testicular sperm (TS), and epididymal sperm (S). An anti-ADAM2 antibody was used as a control.  
 B Expression of SPATC1L in human testis lysates (TL) and mature sperm (S). An anti- $\alpha$ -tubulin antibody was used as a control.  
 C Developmental expression pattern of SPATC1L in testis, examined by immunoblotting using total lysates obtained from prepubertal and adult male mice (days 7, 14–21, 28, 35, 42, 49, and 56). An anti- $\alpha$ -tubulin antibody was used as a control.  
 D Localization of SPATC1L in germ cells during spermatogenesis. Isolated spermatogenic cells were immunostained for SPATC1L (red) and  $\gamma$ -tubulin (green).  $\gamma$ -Tubulin was used as a centrosome marker, and cells were counterstained with the nuclear dye Hoechst 33342 (blue). Fluorescence images of individual staining are shown at the top, and merged images are shown in the middle. Insets are magnified images. Sc, spermatocyte; RS, round spermatid; ES, elongating spermatid; TS, testicular sperm; MS, epididymal mature sperm; BF, overlay with bright-field image. Scale bar = 5  $\mu$ m.

Source data are available online for this figure.

in testicular cells, where SPATC1L was not expressed (Fig 2E). SPATC1L and RI $\alpha$  appeared to co-localize in round spermatids, but not in elongating spermatids. Finally, SPATC1L and RI $\alpha$  were observed to co-localize at the connecting piece in testicular sperm.

**SPATC1L increases PKA activity through binding to RI $\alpha$**

To define precisely the RI $\alpha$  subdomains involved in interaction with SPATC1L, we mapped the binding sites of RI $\alpha$ . To this end, we performed an *in vitro* binding assay using a GST fusion protein containing the entire region of SPATC1L; a GST-only protein was used as a negative control. For RI $\alpha$ , we generated His-fused full-length RI $\alpha$  (amino acids, 1–381) and its serial-deletion mutants, including RI $\alpha$  1 (amino acids 1–136), RI $\alpha$  2 (amino acids 137–253), and RI $\alpha$  3 (amino acids 255–381), which contain the dimerization domain and inhibitor sequence, domain A, and domain B,

respectively (Fig 3A) [22]. In this assay, we found that full-length RI $\alpha$ , but not RI $\alpha$  1, RI $\alpha$  2, or RI $\alpha$  3, interacted with SPATC1L (Fig 3B). Because none of the RI $\alpha$  1–3 mutant proteins associated with SPATC1L, we designed the additional deletion mutants, RI $\alpha$  4 (amino acids 1–253) and RI $\alpha$  5 (amino acids 137–381), which correspond to RI $\alpha$  1 + 2 and RI $\alpha$  2 + 3 regions, respectively (Fig 3A). The RI $\alpha$  4 mutant protein containing the dimerization domain, inhibitor sequence, and domain A bound to SPATC1L, whereas RI $\alpha$  5 did not (Fig 3B). To determine whether SPATC1L binds to the dimerization domain or the C-subunit binding site, we created an RI $\alpha$  4 variant lacking the dimerization domain, designated RI $\alpha$  6 (amino acids 64–253) (Fig 3A). Although SPATC1L was unable to bind to domain A only, it did bind to RI $\alpha$  6, suggesting that SPATC1L binds to the C-subunit binding site in RI $\alpha$ , and further implying that the entire region of the C-subunit binding site is required for association with SPATC1L (Fig 3B).

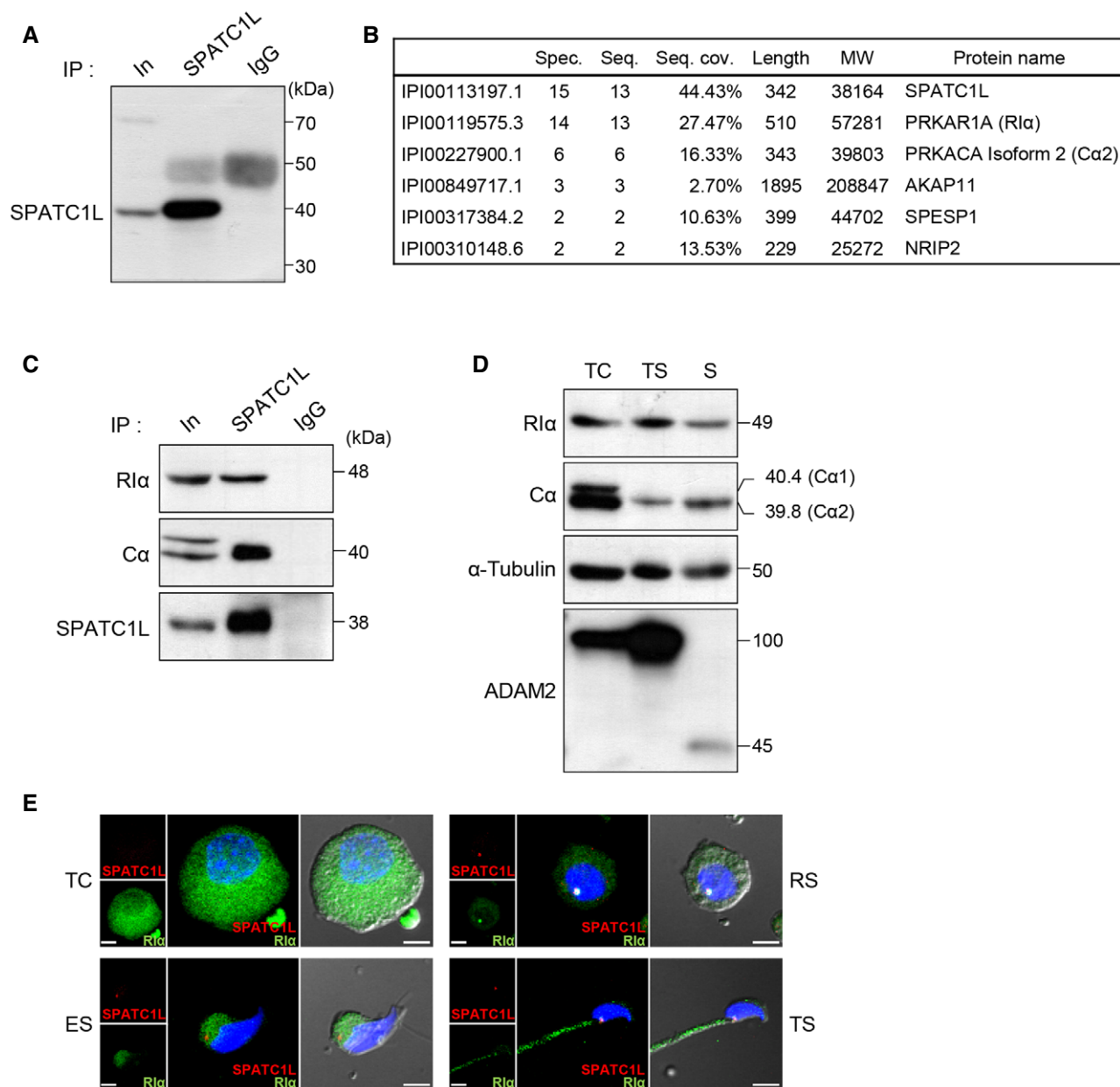


**Figure 2. Identification of SPATC1L-interacting proteins.**

A Immunoprecipitation of SPATC1L in the testis using an anti-SPATC1L antibody. IgG was used as a control. In, input; IgG, normal rabbit serum.

B Proteins associated with SPATC1L, identified by LC-MS/MS analysis. Proteins immunoprecipitated by an anti-SPATC1L antibody were analyzed by LC-MS/MS. Spec., spectrum count; Seq., sequence count (number of non-redundant peptides identified for each protein); Seq. cov., sequence coverage calculated based on the amino acid count; MW, molecular weight calculated using TurboSEQUEST software.

C Interaction between SPATC1L and PKA subunits. Samples precipitated with an anti-SPATC1L antibody were analyzed by immunoblotting with anti-R1 $\alpha$  and anti-C $\alpha$  antibodies. Immunoprecipitation of SPATC1L was confirmed by immunoblotting with anti-SPATC1L antibody. IgG was used as a control. IP, immunoprecipitation; In, input; IgG, immunoglobulin G from normal rabbit serum.

D Expression of PKA subunits during spermatogenesis, examined by immunoblotting for R1 $\alpha$  and C $\alpha$  in testicular cells (TC), testicular sperm (TS), and epididymal sperm (S). Anti-ADAM2 and anti- $\alpha$ -tubulin antibodies were used as controls.

E Localization of SPATC1L and R1 $\alpha$  during spermatogenesis. Isolated spermatogenic cells were immunostained for SPATC1L (red) and R1 $\alpha$  (green), and counterstained with the nuclear dye Hoechst 33342 (blue). Overlay with bright-field image is shown on the right of each cell type. TC, testicular cell (spermatocyte); RS, round spermatid; ES, elongating spermatid; TS, testicular sperm. Scale bar = 5  $\mu$ m.

Source data are available online for this figure.

PKA activity is mainly dependent on cAMP-mediated dissociation of the C-subunit from the R subunit. To investigate whether binding of SPATC1L to R1 $\alpha$  regulates PKA activity, we performed *in vitro*

PKA activity assays by overexpressing SPATC1L in a cell line (TM4) that endogenously expresses R1 $\alpha$  and C $\alpha$ , but not SPATC1L (Fig EV2E). Immunoprecipitation followed by immunoblotting for



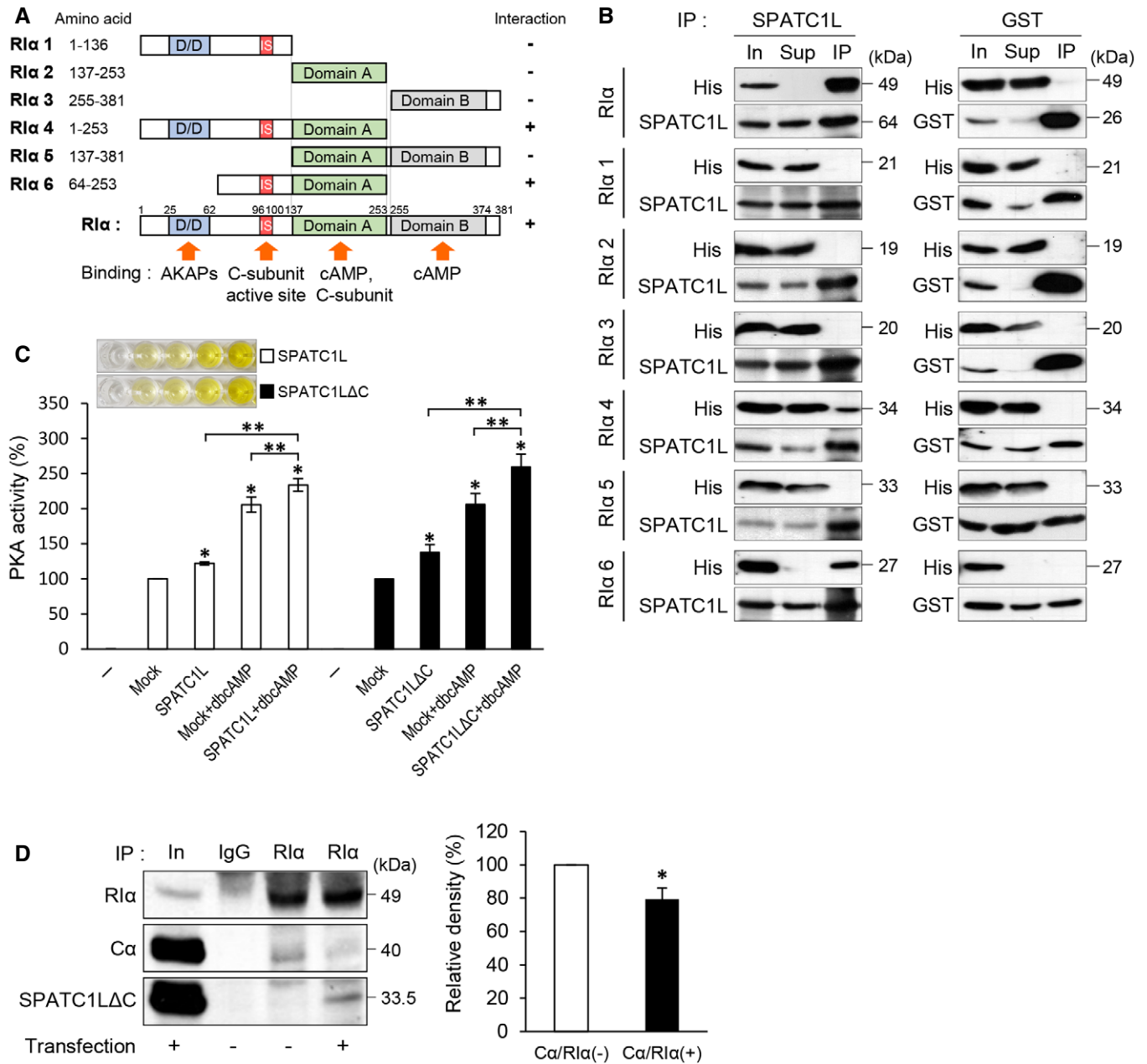


**Figure 3. Interaction between SPATC1L and R1α, and PKA activity.**

**A** Schematic diagrams of R1α regions subjected to *in vitro* binding assays. Results from the R1α-SPATC1L interaction assay (**B**) are indicated as + or – at right. D/D, dimerization/docking domain (binding site for AKAPs); Domain A, catalytic subunit binding domain and cAMP binding domain; Domain B, cAMP binding domain; IS, inhibitor sequence (binding site for the active site of the catalytic subunit).

**B** Mapping of the SPATC1L binding site on R1α by *in vitro* binding assay using purified GST-SPATC1L and His-R1α proteins consisting of regions 1–6. Purified GST protein only was used as a control. Binding was confirmed by immunoprecipitation using an anti-SPATC1L antibody followed by immunoblot analyses of R1α, detected using an anti-His antibody. In, input; Sup, supernatant; IP, immunoprecipitated protein.

**C** PKA activity after overexpression of SPATC1L or SPATC1LΔC. Graphs show the average PKA activity of *Spac11*-transfected cells (white bar) and *Spac11ΔC*-transfected cells (black bar) in the presence or absence of cAMP, expressed relative to control cells (mock) as a percentage. Representative signals observed in the assay are shown above. The overexpression of SPATC1L was confirmed in every experiment by immunoblotting (data not shown). Data are presented as means ± SD ( $n > 3$ ; \* $P < 0.05$  versus mock, \*\* $P < 0.01$ , Student's *t*-test).

**D** The amount of Cα associated with R1α in the presence or absence of SPATC1LΔC. After IP of R1α in cells overexpressing SPATC1LΔC or control, immunoblot analysis was performed using anti-Cα antibody. Graph shows densitometric analysis of Cα in relation to immunoprecipitated R1α in immunoblot analysis. In, input; IgG, immunoglobulin G from normal rabbit serum. Data are presented as means ± SD ( $n = 3$ ; \* $P < 0.05$ , Student's *t*-test).

Source data are available online for this figure.

RI $\alpha$  confirmed that SPATC1L interacted with RI $\alpha$  after transfection in this cell line (Fig EV2F). The PKA activity was determined by measuring the phosphorylation levels of PKA-specific substrates incubated with lysates from the cell line. As shown in Fig 3C, expression of SPATC1L led to a modest (~21%), but significant, increase in PKA activity compared with control cells (100% in mock versus ~121.8% in SPATC1L; Fig 3C). Further, we performed *in vitro* PKA activity assays by overexpressing SPATC1L lacking the N-terminal coiled-coil domain (SPATC1L $\Delta$ C). SPATC1L $\Delta$ C interacted with RI $\alpha$ , suggesting that the coiled-coil region of SPATC1L was not required for interaction with RI $\alpha$  (Fig EV2G). Similarly, we found increased PKA activity in cells overexpressing SPATC1L $\Delta$ C (~37%), suggesting that a region besides the coiled-coil domain regulates PKA activity (Fig 3C). The PKA activity was also increased in cell-permeable cAMP analogue dibutyryl cAMP (dbcAMP)-treated cells. This increase in PKA activity was further enhanced by SPATC1L (~27.9%) and SPATC1L $\Delta$ C (~53.7%), compared with control cells (mock+dbcAMP) (Fig. 3C). To determine whether binding of SPATC1L to the C-subunit binding site in RI $\alpha$  increased PKA activity, we compared the amounts of C $\alpha$  associated with RI $\alpha$  in the presence or absence of SPATC1L. The amount of C $\alpha$  associated with RI $\alpha$  was significantly decreased (~24%) in the presence of SPATC1L compared with control (Fig 3D). Collectively, these results suggest that SPATC1L interacts with the C-subunit binding site of RI $\alpha$  and competitively inhibits the association between RI $\alpha$  and C $\alpha$ , thereby increasing the kinase activity of PKA.

### Male mice lacking SPATC1L are infertile

The dynamics of SPATC1L expression during spermiogenesis indicated that SPATC1L might play a functional role in sperm development. We examined the possibility of SPATC1L as a regulator of cilia formation by overexpressing the protein in cultured cells. We found that the protein did not regulate ciliogenesis or ciliary length *in vitro* (Fig EV2H and I). To investigate the *in vivo* function of SPATC1L in male reproduction, we generated knockout mice (KO) using CRISPR/Cas9 genome editing. To disrupt *Spatc1l*, we designed guide RNAs (gRNAs) targeting the start codon in exon 1. These gRNAs, together with Cas9 mRNA, were then injected into mouse zygotes to allow gRNAs to lead Cas9 to cleave target sites in mouse embryos. After injection, these CRISPR/Cas9-injected zygotes were transplanted into foster mothers. We ultimately obtained 52 founder mice, 10 of which were confirmed through Sanger sequencing to exhibit CRISPR/Cas9 targeting and repair by non-homologous end joining (Fig EV3A). For phenotypic analyses, we selected a single mouse line that contained a deletion mutation of the start codon in exon 1 of *Spatc1l*, and crossed this founder mouse with wild-type (WT) C57BL/6J; the resulting heterozygotes were interbred to obtain homozygous *Spatc1l*<sup>-/-</sup> mice (Fig 4A). An examination of *Spatc1l* mRNA and protein in testes confirmed the generation of WT (*Spatc1l*<sup>+/+</sup>), heterozygous (*Spatc1l*<sup>+/-</sup>), and homozygous (*Spatc1l*<sup>-/-</sup>) KO mice. The homozygous KO mice were found to completely lack *Spatc1l* mRNA and protein in testis (Fig 4B and C). It should be noted that the amount of SPATC1L was reduced in heterozygous mice.

The weights and growth rates of *Spatc1l*<sup>-/-</sup> mice were not significantly different from those of WT mice. To determine whether loss of SPATC1L affects reproductive functions, we performed a fertility

test. Although all adult female *Spatc1l*<sup>-/-</sup> mice were fertile, adult male *Spatc1l*<sup>-/-</sup> mice were unable to induce pregnancy in WT females and did not produce pups after mating with WT females, despite frequent observations of vaginal plugs in the females (Fig 4D and E). These results indicate that *Spatc1l*<sup>-/-</sup> male mice are sterile. Moreover, the percentage of pregnant females (22%), average litter size (0.58  $\pm$  0.2), and fertility rate (~7.71%) for *Spatc1l*<sup>+/-</sup> male mice were also significantly reduced compared with that for WT males (83%, 7.56  $\pm$  0.8, 100%), indicating haploinsufficiency of SPATC1L in fertility (Fig 4D and E). It should be noted that *Spatc1l*<sup>+/-</sup> mice showed reduced levels (~47%) of SPATC1L protein in testes (Fig 4C). These data suggest that a *Spatc1l* deficiency compromises male fertility and that severity of this phenotype depends on the amount of SPATC1L protein.

### Loss of SPATC1L leads to tailless and acephalic sperm

To uncover the cause of the male sterility phenotype, we first examined testes from adult *Spatc1l*-KO mice. No significant differences in testis size or testis-to-body-weight ratio were observed between WT and KO mice (Fig 5A and B). We also found that the appearance and weight of the epididymis from KO mice were comparable to those from WT mice (Fig 5C and D). Moreover, histological analyses revealed no disruptions in seminiferous tubules in adult KO testis (Fig 5E). To further investigate the phenotype of KO mice, we evaluated mature sperm collected from the cauda epididymis and vas deferens of WT, heterozygous, and KO mice. An analysis of sperm revealed no significant differences in sperm head counts between WT, heterozygous, and KO mice (Fig 5F). However, further microscopic analyses revealed morphological abnormalities in almost all of the sperm from *Spatc1l*-KO mice (Fig 5G and H). Immunofluorescence staining using an anti- $\alpha$ -tubulin antibody in conjunction with Hoechst nuclear staining revealed that heads were separated from tails in most cauda epididymal sperm from KO mice and detached heads were abnormally located to the midpiece region of sperm flagella in some sperm (~10%) from KO mice (Fig 5I). We also found that cauda epididymides of heterozygous (*Spatc1l*<sup>+/-</sup>) mice contained both headless sperm (~53%) and sperm with folded heads (~25%) (Figs 5G and H, and EV3B). This phenotype was also observed in heterozygous mice generated from another KO founder (#35), confirming the haploinsufficiency of SPATC1L (Fig EV3C and D). Although we did not detect any intact sperm in the cauda epididymis from KO mice, we obtained some normal testicular sperm from KO testes (Fig EV3E). Quantitative analyses revealed that intact testicular sperm accounted for ~21% of the total sperm population in KO testes, implying that disengagement of heads from tails occurs during sperm development in the testis as well as during maturation in the epididymis. Interestingly, ~79% of headless flagella from the KO cauda epididymis exhibited motility, albeit weaker than that of WT epididymal sperm (Movies EV1–EV3). Finally, we also observed separation of heads from tails in all of the ejaculated sperm obtained from the uterus of WT females mated with KO males. Taken together, these results demonstrate that loss of SPATC1L results in the formation of abnormal sperm, including acephalic and headless sperm, possibly owing to instability in the head-tail junction, thereby leading to male sterility.

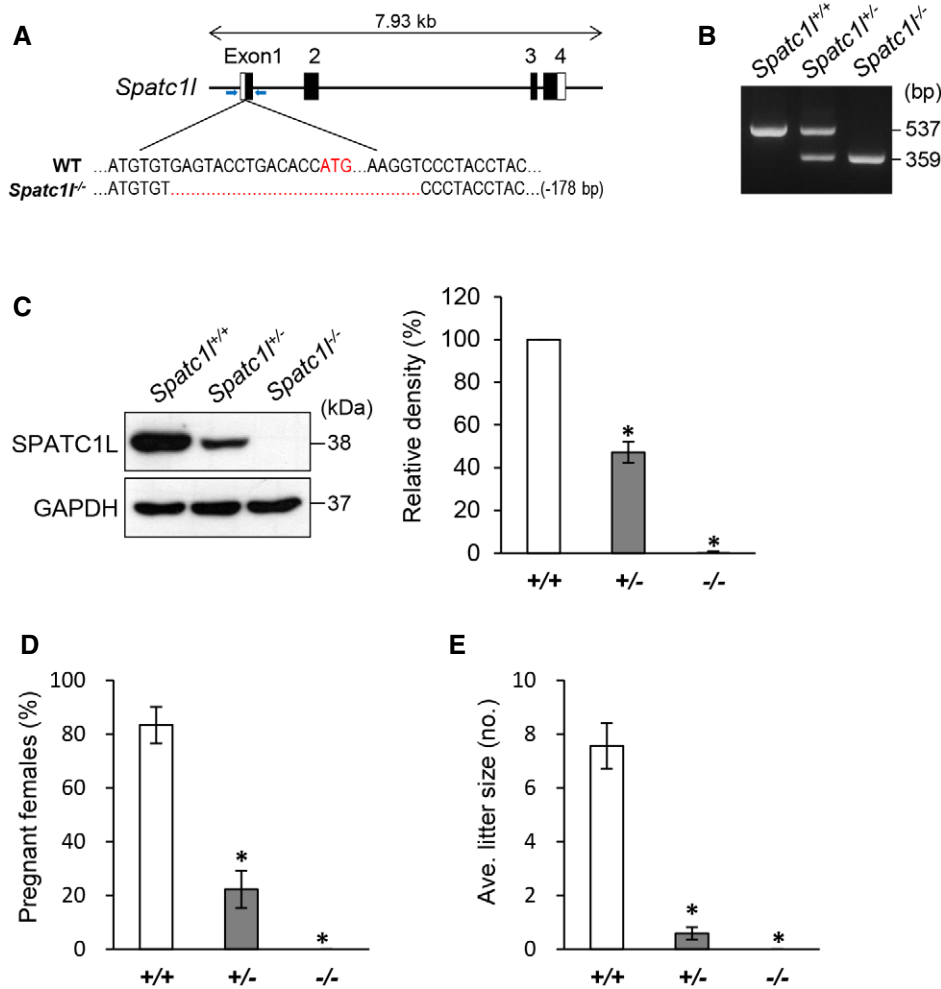


**Figure 4. Generation of *Spatc1*-KO mice and assessment of male fertility.**

**A** Schematic diagram of the *Spatc1* gene coding region and region deleted using CRISPR/Cas9. The start codon sequence is labeled in red. Blue arrows indicate the forward and reverse primers used for genotyping. The numbers in boxes indicate exons, and filled boxes show *Spatc1* coding regions. The 178-bp sequence deleted in the targeted allele of a *Spatc1*<sup>-/-</sup> mouse (red dots) is indicated in partial sequencing results, shown below.

**B** PCR genotyping analysis of WT (*Spatc1*<sup>+/+</sup>), heterozygous (*Spatc1*<sup>+/-</sup>), and homozygous (*Spatc1*<sup>-/-</sup>) mice.

**C** SPATC1L expression levels in testes obtained from WT, *Spatc1*<sup>+/-</sup>, and *Spatc1*<sup>-/-</sup> mice. An anti-GAPDH antibody was used as a control. Graph shows densitometric analysis of SPATC1L in relation to GAPDH in immunoblot analysis. Data are presented as means ± SD (n = 3, \*P < 0.001, Student's t-test).

**D** Percentage of females that became pregnant after mating with WT (white bar), *Spatc1*<sup>+/-</sup> (gray bar), and *Spatc1*<sup>-/-</sup> (black bar) male mice. Male mice used: WT, n = 5; *Spatc1*<sup>+/-</sup>, n = 6; *Spatc1*<sup>-/-</sup>, n = 7. WT female mice used for mating with the indicated genotype: WT, n = 30; *Spatc1*<sup>+/-</sup>, n = 36; *Spatc1*<sup>-/-</sup>, n = 42. Vaginal plugs were observed in all mated females. Data are presented as means ± SD (\*P < 0.001, Student's t-test).

**E** Average litter size of pups produced by females mated with WT (white bar), *Spatc1*<sup>+/-</sup> (gray bar), and *Spatc1*<sup>-/-</sup> (black bar) male mice. The numbers of used male and female mice are the same as those in (D). Data are presented as means ± SD (\*P < 0.001, Student's t-test).

Source data are available online for this figure.

### Loss of SPATC1L does not affect the development of the connecting piece, but alters head-tail integrity

To further define the morphology of KO sperm, we observed their fine structures by scanning electron microscopy (SEM). This analysis revealed that separation of heads from tails occurred below the postacrosomal region of the sperm heads (Fig 6A). The shapes of severed surface in headless flagella were uniform among sperm. In previous results, although all cauda epididymal KO sperm were acephalic, some testicular sperm was intact in KO mice (Fig EV3E). To determine whether loss of SPATC1L causes structural defects

during spermiogenesis, we investigated the ultrastructure of testicular and epididymal sperm by transmission electron microscopy (TEM), first examining cross-sections of the *Spatc1* KO sperm flagellum. This analysis showed that KO testicular sperm had a well-defined mitochondrial sheath, normally arranged outer dense fibers, and an axoneme with a normal “9 + 2” microtubule structure in the midpiece (Fig 6B). The end piece of KO testicular sperm also consisted of a “9 + 2” axonemal microtubule organization, indicating that flagella formation occurs normally in KO testicular sperm. We also analyzed longitudinal sections of WT and KO elongating spermatids and testicular sperm. There were no differences in

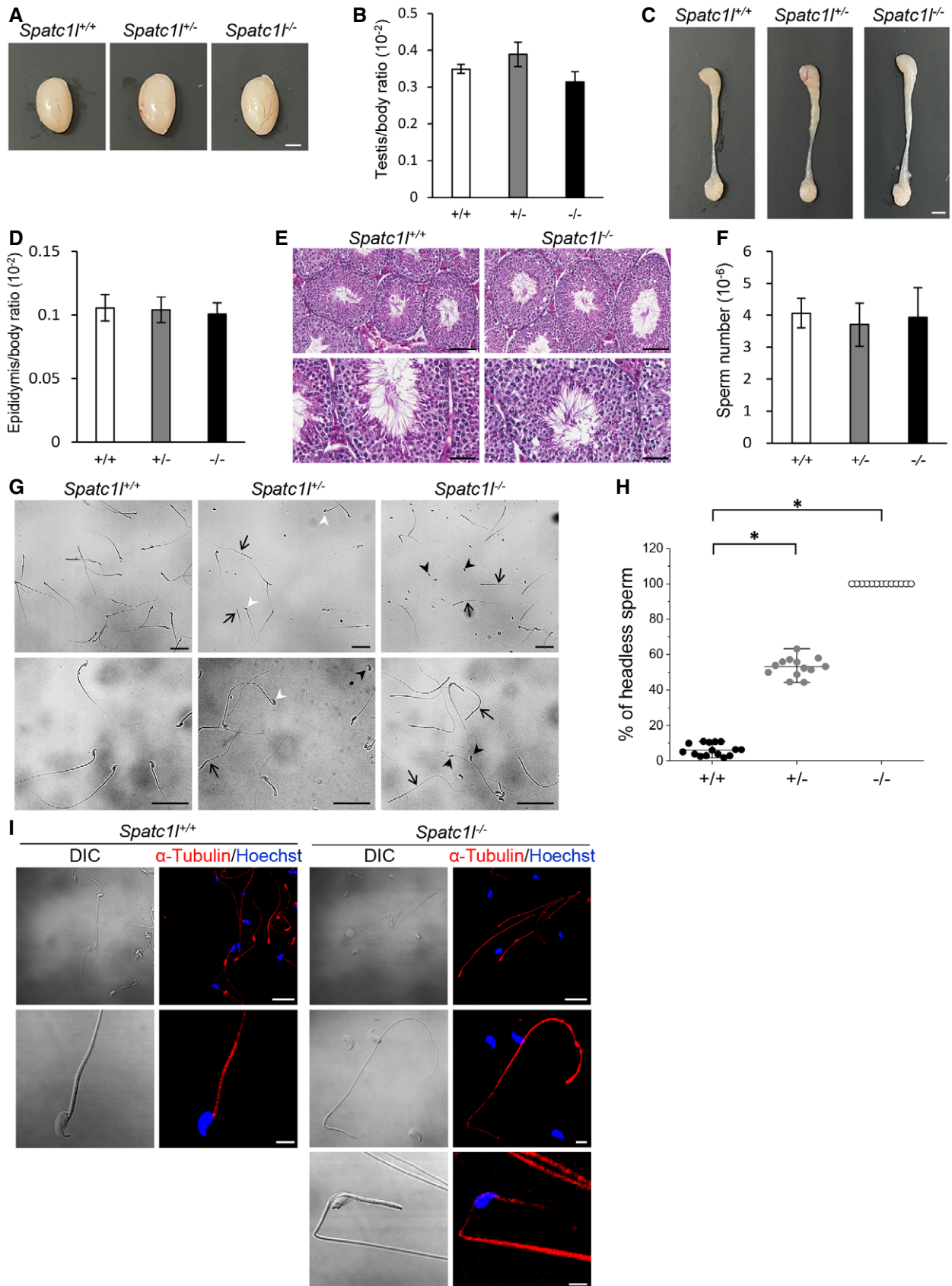


Figure 5.



**Figure 5. Phenotypic analyses of *Spatc1l*-KO mice.**

- A Macroscopic appearance of adult testes from 8-week-old WT (*Spatc1l*<sup>+/+</sup>), heterozygous (*Spatc1l*<sup>+/-</sup>) and homozygous (*Spatc1l*<sup>-/-</sup>) mice. Scale bar = 2 mm.
- B Comparison of testis weight in WT (white bar), *Spatc1l*<sup>+/-</sup> (gray bar), and *Spatc1l*<sup>-/-</sup> (black bar) mice. The organs were trimmed of fat and weighed. The average testis weight/body weight ratios for WT, *Spatc1l*<sup>+/-</sup>, and *Spatc1l*<sup>-/-</sup> males were 0.0034 ± 0.0001, 0.0038 ± 0.0003, and 0.0031 ± 0.0002, respectively. Data are presented as means ± SD (n = 7).
- C Macroscopic appearance of the adult epididymis from WT, *Spatc1l*<sup>+/-</sup>, and *Spatc1l*<sup>-/-</sup> mice. Scale bar = 2 mm.
- D Epididymis weight in WT (white bar), *Spatc1l*<sup>+/-</sup> (gray bar), and *Spatc1l*<sup>-/-</sup> (black bar) mice. The average epididymis weight/body weight ratios for WT, *Spatc1l*<sup>+/-</sup>, and *Spatc1l*<sup>-/-</sup> males were 0.001 ± 0.0001, 0.001 ± 0.0001, and 0.001 ± 0.00008, respectively. Data are presented as means ± SD (n = 7).
- E Histological analysis of hematoxylin and eosin-stained sections of seminiferous tubules prepared from testes of WT and KO mice. Scale bar = 100 μm (upper) and 50 μm (lower).
- F Number of mature epididymal sperm from WT (white bar), *Spatc1l*<sup>+/-</sup> (gray bar), and *Spatc1l*<sup>-/-</sup> (black bar) mice. Sperm were collected from the vas deferens. The average number of mature sperm in WT, *Spatc1l*<sup>+/-</sup>, and *Spatc1l*<sup>-/-</sup> males was (4.06 ± 0.40) × 10<sup>6</sup>, (3.7 ± 0.7) × 10<sup>6</sup>, and (3.93 ± 0.90) × 10<sup>6</sup>, respectively. Data are presented as means ± SD (n = 5).
- G Morphological analyses of epididymal sperm in WT, He, and KO mice. Epididymal sperm were observed under an inverted microscope. The arrows indicate separated tails, black arrowheads indicate separated heads, and white arrowheads indicate folded heads. Scale bar = 50 μm.
- H Percentage of headless sperm from cauda epididymides of WT (black), *Spatc1l*<sup>+/-</sup> (gray), and *Spatc1l*<sup>-/-</sup> (white) mice. The average percentage of headless sperm in WT, *Spatc1l*<sup>+/-</sup>, and *Spatc1l*<sup>-/-</sup> males was 6.3, 52.9, and 100, respectively. Each dot represents percentage of headless sperm in an individual mouse, and medians are represented as horizontal lines (n = 13, \*P < 0.001, Student's t-test).
- I Immunostaining analysis of sperm heads and tails in WT and KO mice. Sperm tails were observed by immunostaining for α-tubulin antibody (red), and counterstaining with the nuclear dye Hoechst 33342 (blue). Sperm were also observed by differential interference contrast (DIC) microscopy. Scale bars = 20 μm (upper) and 5 μm (lower).

structural development in elongating spermatids between WT and KO mice during spermiogenesis. The nucleus, manchette, and connecting piece (consisting of segmented columns and basal plate), as well as the annulus located at the distal end of the midpiece, all formed normally in both WT and KO mice (Fig 6C). In addition, a TEM analysis of longitudinal sections of testicular sperm revealed no discernable defects in formation of the connecting piece in the KO compared with the WT. The connecting piece of *Spatc1l*-KO testicular sperm consisted of a basal plate that was normally attached to the nuclear envelope, and well-arranged capitulum and segmented columns (Fig 6C).

Because we found that sperm heads were separated from tails in the KO cauda epididymis, we further investigated the ultrastructure of KO epididymal sperm. This analysis showed that the structure of the basal plate was maintained in separated heads of *Spatc1l*-KO cauda epididymal sperm, whereas the capitulum and segmented column were found in the separated tail rather than the cytoplasm of the head (Fig 6D). These results strongly suggest that head-tail separation of KO sperm occurs between the basal plate and capitulum, with subsequent sealing of both head and tail stumps by the plasma membrane. Interestingly, the TEM analysis of the KO cauda epididymis revealed a head detached from the connecting piece that was abnormally associated with the midpiece of the sperm flagellum, as also observed by differential interference (DIC) confocal microscopy (Fig 6E). These images suggest that the separated head is positioned within the same plasma membrane that encloses the midpiece. Collectively, these results demonstrate that loss of SPATC1L does not affect structural development of the connecting piece, and suggest that sperm heads slip down from the tails spontaneously or the flagella push past the detached heads during sperm development and/or maturation because of reduced head-tail junction affinity caused by the loss of SPATC1L.

#### **CAPZB is a potential target of PKA-mediated phosphorylation in the neck region of testicular sperm**

In this study, we found that SPATC1L interacts with RIα (see Fig 3). The loss of SPATC1L did not affect the expression level of RIα in

testis or epididymal sperm (Fig EV4A and B), or the localization of RIα and AKAP11 during spermatogenesis, suggesting that the localization of RIα is dependent on AKAP11 and not influenced by SPATC1L (Fig EV4C and D). To determine whether the phenotype of *Spatc1l*-KO mice is related to a change in PKA activity, we measured and compared PKA kinase activity in WT and KO testicular sperm. This analysis revealed that PKA activity in KO testicular sperm was ~87.47% of that in WT testicular sperm, a modest but significant decrease (Fig 7A). The weak decline of the PKA activity is likely due to limited SPATC1L occupation in spermatogenic cells and testicular sperm in which most PKA is not affected by the absence of SPATC1L in activity. We suggest that loss of SPATC1L may cause a reduction in PKA activity at the connecting piece of testicular sperm, leading to separation of head and tail.

Because the molecules involved in the sperm head-tail junction affinity are unknown, we sought to identify proteins whose phosphorylation was altered by a deficiency of PKA activity in the connecting piece. To accomplish this, we separated WT and KO testis total proteins by two-dimensional gel electrophoresis (2DE), and detected phosphorylation using ProQ Diamond staining. In this analysis, we selected a total of five spots that showed a significant difference in the degree of phosphorylation between WT and KO testis (Fig 7B). The phosphorylation levels of all selected spots were significantly decreased in *Spatc1l*-KO compared with WT testis (Fig 7C). A subsequent peptide mass fingerprinting (PMF) analysis of the selected spots identified five proteins (Fig 7D): EFHD2 (EF hand domain containing 2), SRSF1 (serine/arginine-rich splicing factor 1), CAPZB, SERPINB6A (serine peptidase inhibitor, clade B, member 6a), and ERLIN2 (ER lipid raft associated 2). To further explore the expression of these proteins in testis and epididymal sperm, we performed an immunoblot analysis. This analysis revealed that all five proteins were expressed in testes at similar levels in WT and KO mice, suggesting that the loss of *Spatc1l* does not affect the expression levels of these proteins (Fig 7E). Only three proteins (SRSF1, CAPZB, and ERLIN2) were expressed in epididymal sperm, suggesting that these proteins are potentially involved in maintaining the integrity of the sperm neck (Fig 7F). A further investigation of the localization of these three proteins in testicular

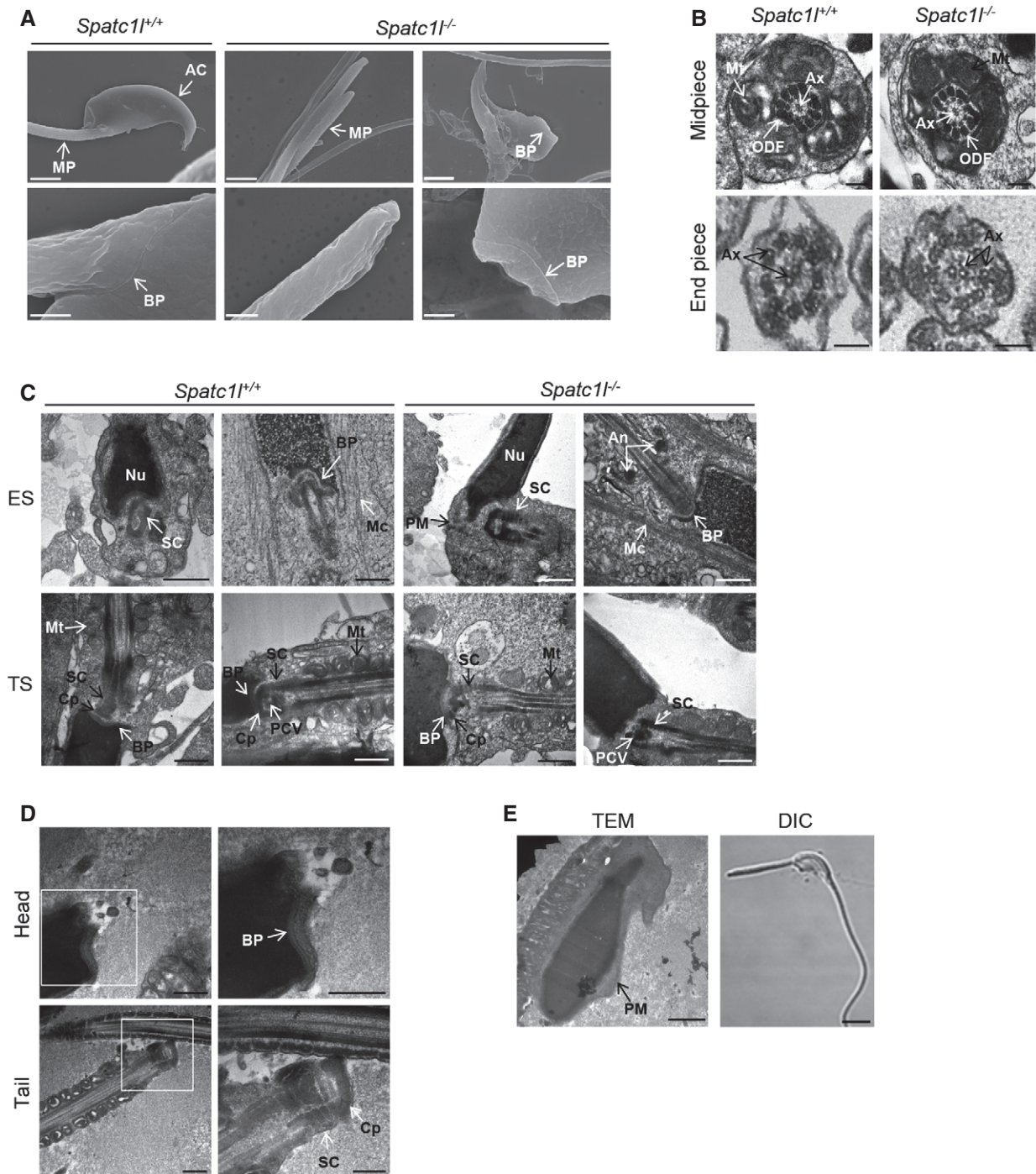


**Figure 6. Ultrastructures of sperm in *Spatc1*-KO mice.**

**A** Morphological analyses of *Spatc1*-KO epididymal sperm by SEM. Sperm were obtained from the vas deferens of 8-week-old WT (*Spatc1*<sup>+/+</sup>) and KO (*Spatc1*<sup>-/-</sup>) mice. Sperm neck regions are magnified in lower panels. AC, acrosomal cap; MP, midpiece; BP, basal plates. Scale bar = 2  $\mu$ m (upper) and 0.5  $\mu$ m (lower).

**B** TEM analyses of flagella in WT and KO testicular sperm. TEM images represent ultrastructures of cross-sections of the midpiece (upper) and end piece (lower) of WT and KO testicular sperm. Ax, axonemal microtubules; Mt, mitochondrial sheath; ODF, outer dense fibers. Scale bars = 200 nm (upper) and 100 nm (lower).

**C** TEM analyses of the development of the connecting piece in WT (left) and KO (right) sperm. TEM images represent ultrastructures of longitudinal sections of elongating spermatids (ES) and testicular sperm (TS) in WT and KO mice. An, annulus; BP, basal plates; Cp, capitulum; Mc, manchette; Mt, mitochondria; Nu, nucleus; PCV, proximal centriolar vault; PM, plasma membrane; SC, segmented column. Scale bar = 500 nm.

**D** Ultrastructures of epididymal sperm in KO mice. TEM images represent ultrastructures of separated sperm head (upper) and tail (lower) in the epididymis of KO mice. Images in the boxes are enlarged at right. BP, basal plates; Cp, capitulum; SC, segmented column. Scale bar = 500 nm.

**E** TEM analysis of morphologically abnormal KO sperm. Detached heads abnormally located to the midpiece of sperm flagella were observed by TEM (left) and confocal differential interference contrast (DIC) microscopy (right). PM, plasma membrane. Scale bars = 500 nm (left) and 5  $\mu$ m (right).

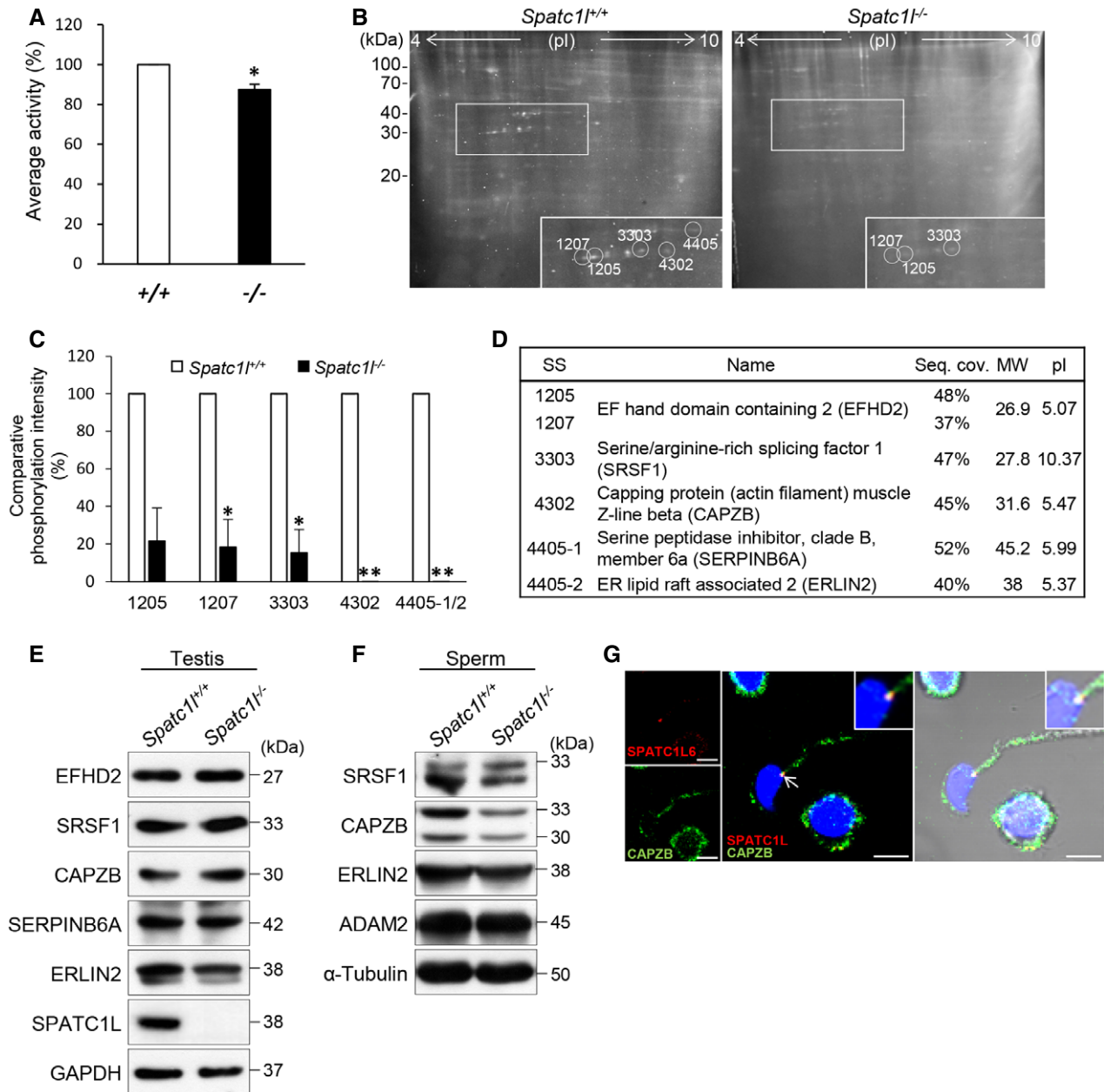


**Figure 7. Identification of CAPZB as a candidate target of phosphorylation by PKA in the neck region of testicular sperm.**

- A** PKA activities in testicular sperm from WT (+/+) and KO (-/-) mice. Graph shows average PKA activity in testicular sperm from KO mice (black bar) relative to that from WT mice (white bar), expressed as a percentage. Data are presented as means  $\pm$  SD ( $n = 3$ ; \* $P < 0.05$ , Student's  $t$ -test).
- B** Representative ProQ Diamond-stained 2D gel images of isolated proteins from testes in WT (left) and KO (right) mice. Testes lysates were separated by 2DE, and phosphoproteins were stained with ProQ diamond. Images in the boxes are enlarged in insets shown below. Circles with numbers indicate spots with significantly changed volume relative to those on WT gels.
- C** Comparative phosphorylation intensities of selected spots in 2D gels. The intensities of selected spots in KO gels were compared with intensities in WT gels. Average intensities of the indicated spot numbers (#) in WT (white bar) and KO (black bar): #1205, 1092.2 (WT) and 244.98 (KO); #1207, 729.9 (WT) and 140.43 (KO); #3303, 1165.5 (WT) and 279.5 (KO); #4302, 2725.8 (WT) and 1 (KO); #4405, 984.5 (WT) and 1 (KO). An intensity value of 1 indicates no spot, but is provided for calculation of fold change. Data are presented as means  $\pm$  SD ( $n = 3$ ; \* $P < 0.05$ , \*\* $P < 0.001$ , Student's  $t$ -test).
- D** Identification of proteins with altered phosphorylation patterns in *Spatc1*-KO testis by PMF. SS, standard spot; Seq. cov., sequence coverage calculated based on the amino acid count; MW, molecular weight; pI, isoelectric point.
- E, F** Immunoblot analyses of five candidate proteins in testis (E) and sperm (F) of WT and KO mice. Anti-GAPDH, anti-ADAM2, and anti- $\alpha$ -tubulin antibodies were used as controls. Loss of SPATC1L in KO testis was confirmed by immunoblotting with anti-SPATC1L antibody.
- G** Localization of SPATC1L (red) and CAPZB (green) in testicular sperm. Overlay with bright-field image is shown at right. The white arrow indicates the spatial overlap between SPATC1L and CAPZB. Scale bar = 5  $\mu$ m.

Source data are available online for this figure.



**Figure 8. Characterization of phosphorylation in CAPZB by PKA.**

- A The amount of CAPZB in mature sperm from WT (+/+) and KO (−/−) mice. Graph shows densitometric analysis of CAPZB shown in immunoblot analyses (Fig 7F), expressed relative to WT as a percentage. The density of CAPZB in immunoblot analysis was calculated in relation to density of  $\alpha$ -tubulin. Data are presented as means  $\pm$  SD ( $n = 3$ , \* $P < 0.001$ , Student's  $t$ -test).
- B The amount of CAPZB in mock and *Spac11Lac*-transfected cells. Anti-GAPDH antibody was used as control. Overexpression of SPATC1L in TM4 cells was confirmed by immunoblotting with anti-SPATC1L antibody. Graph shows densitometric analysis of CAPZB in pcDNA3.1 vector-transfected control cells (mock; white bar) and SPATC1LAC-transfected cells (black bar), expressed relative to control cells (mock) as a percentage. The density of CAPZB in immunoblot analysis was calculated in relation to density of GAPDH. Data are presented as means  $\pm$  SD ( $n = 3$ , \* $P < 0.001$ , Student's  $t$ -test).
- C Phosphorylation of CPAZB3 by cAMP-dependent protein kinase (PKA). CAPZB3 was incubated with PKA and  $^{32}$ P, and estimated by autoradiography. The amount of CAPZB3 protein was quantified by Coomassie Brilliant Blue (CBB) staining (lower).
- D Phosphorylation of CPAZB3 in the presence or absence of SPATC1L. Phosphorylation of purified CAPZB3 was labeled with  $^{32}$ P via PKA in the presence or absence of SPATC1L and estimated by autoradiography. The amount of CAPZB3 protein was quantified by Coomassie Brilliant Blue (CBB) staining (lower). Graph shows densitometric analysis of phospho-CAPZB3 (p-CAPZB3) in reactions without (control; white bar) or with SPATC1L (black bar), expressed relative to control as a percentage. Data are presented as means  $\pm$  SD ( $n = 4$ , \* $P < 0.001$ , Student's  $t$ -test).
- E Observation of filamentous actin (F-actin) in the presence (lower) or absence (upper) of SPATC1L. F-actin in pEGFP vector-transfected control cells (mock; upper, green) and cells overexpressing SPATC1LAC (lower, green) was visualized by staining using phalloidin (red). White bar shows the length of transfected cell. Scale bar = 50  $\mu$ m.
- F The length of cell overexpressing SPATC1LAC compared with control. Graph shows the average of measured cell length in pEGFP vector-transfected control cells (mock; white bar) and *Spac11Lac*-transfected cells (black bar), expressed relative to control cells (mock) as a percentage. Data are presented as means  $\pm$  SD ( $n = 3$ ; \* $P < 0.001$ , Student's  $t$ -test).
- G Proposed model for the function of SPATC1L in maintaining the stability of the sperm head-tail junction. SPATC1L is localized to the centrosome in a round spermatid, but separated from the centrosome in an elongating spermatid. Finally, SPATC1L is localized to the neck region close to the centriole in testicular sperm. SPATC1L acts through interactions with R1 $\alpha$  to increase PKA activity and thereby increases the phosphorylation of CAPZB and stability of F-actin responsible for the integrity of the head-tail junction.

Source data are available online for this figure.

sperm showed that only CAPZB was co-localized with SPATC1L, although partially overlapping, in the neck region (Figs 7G and EV5A and B).

Interestingly, CAPZB levels were significantly lower (~53%) in KO epididymal sperm consisting of separated heads and tails (Figs 7F and 8A). Further immunoblot analyses of *Spac11Lac*-transfected cells also showed that the CAPZB level was significantly increased (~43%) in cells overexpressing SPATC1LAC, suggesting that the amount and/or stability of CAPZB is regulated by SPATC1L (Fig 8B). CAPZB contains numerous, potential serine/threonine phosphorylation sites (<http://www.phosphosite.org/homeAction.action>), two of which (Ser2 and Ser263) were observed to be phosphorylated [23,24]. However, the phosphorylation of CAPZB by PKA has not been reported yet. To determine whether CAPZB is phosphorylated by PKA, we generated GST-tagged CAPZB3, a CAPZB isoform specifically expressed in testis (Fig EV5C) and performed *in vitro* kinase assay. In this assay using PKA holoenzyme, CAPZB3 was clearly phosphorylated by PKA (Figs 8C and EV5D). To further determine whether SPATC1L regulates the phosphorylation of CAPZB3 by PKA, we performed *in vitro* kinase assay in the presence or absence of SPATC1L. As shown in Fig 8D, the degree of CAPZB3 phosphorylation by PKA was significantly increased (~20%) by SPATC1L (Fig 8D). SPATC1L also increased the phosphorylation level of BPDEtide (~28.6%), one of the specific substrates for PKA, confirming that SPATC1L in general increases PKA activity (Fig EV5E). Taken together with the data showing changes in the CAPZB amount by SPATC1L (Fig 8A and B), these results suggest that enhanced phosphorylation of CAPZB by SPATC1L-activated PKA may increase stability and/or activity of CAPZB. CAPZB caps the fast-growing (barbed) end of actin filaments in a calcium-independent manner, thereby blocking actin filament assembly and disassembly at the barbed filament ends. It functions in stabilizing actin filament lengths and regulating actin filament dynamics. To investigate whether F-actin dynamics is regulated by SPATC1L which promotes CAPZB phosphorylation, we examined F-actin

structures of SPATC1L-transfected cells. To increase the effect of SPATC1L which has limited cellular occupation (Fig EV1), we performed transfection analysis using *Spac11Lac*. F-actin staining with phalloidin showed that the lengths of cells overexpressing SPATC1LAC were significantly shorter (~44%) than those of control cells, suggesting that polymerization of F-actin was inhibited (Fig 8E and F). Actin filaments maintain a constant length in a state of dynamic equilibrium where monomer disassembly from the (−) end and polymerization at the (+) end is balanced. Disassembly of actin filaments is tightly controlled by proteins including CAPZB [25,26]. The barbed end capping by CAPZB is essential for efficient disassembly of pointed ends of actin filaments. Thus, our results suggest that CAPZB phosphorylation promoted by SPATC1L-activated PKA shortens actin filaments by blocking monomer addition at the fast-growing end of polymers. Although the role of F-actin in the neck region of sperm is unknown, we suggest CAPZB as a potential protein target of SPATC1L-activated PKA that may be responsible for stabilizing the head-tail junction by regulating the F-actin dynamics during sperm development and maturation (Fig 8G).

## Discussion

Genes specifically expressed in male germ cells are important for successful spermatogenesis. In this study, we investigated the function of the previously identified but uncharacterized protein, SPATC1L, which is expressed solely in male germ cells [8]. SPATC1L is homologous to SPATC1 (a.k.a. speriolin) previously also found to be a male germ cell-specific protein located at the connecting piece region of mouse and human sperm. Unlike SPATC1L, SPATC1 is present in mature sperm and interacts with cell division cycle 20 (CDC20) [27,28]. Thus, SPATC1L function is likely to be different from that of SPATC1 [27,28]. Here, we show for the first time that SPATC1L is localized to the centrosome of round spermatids and to the connecting piece of testicular sperm.



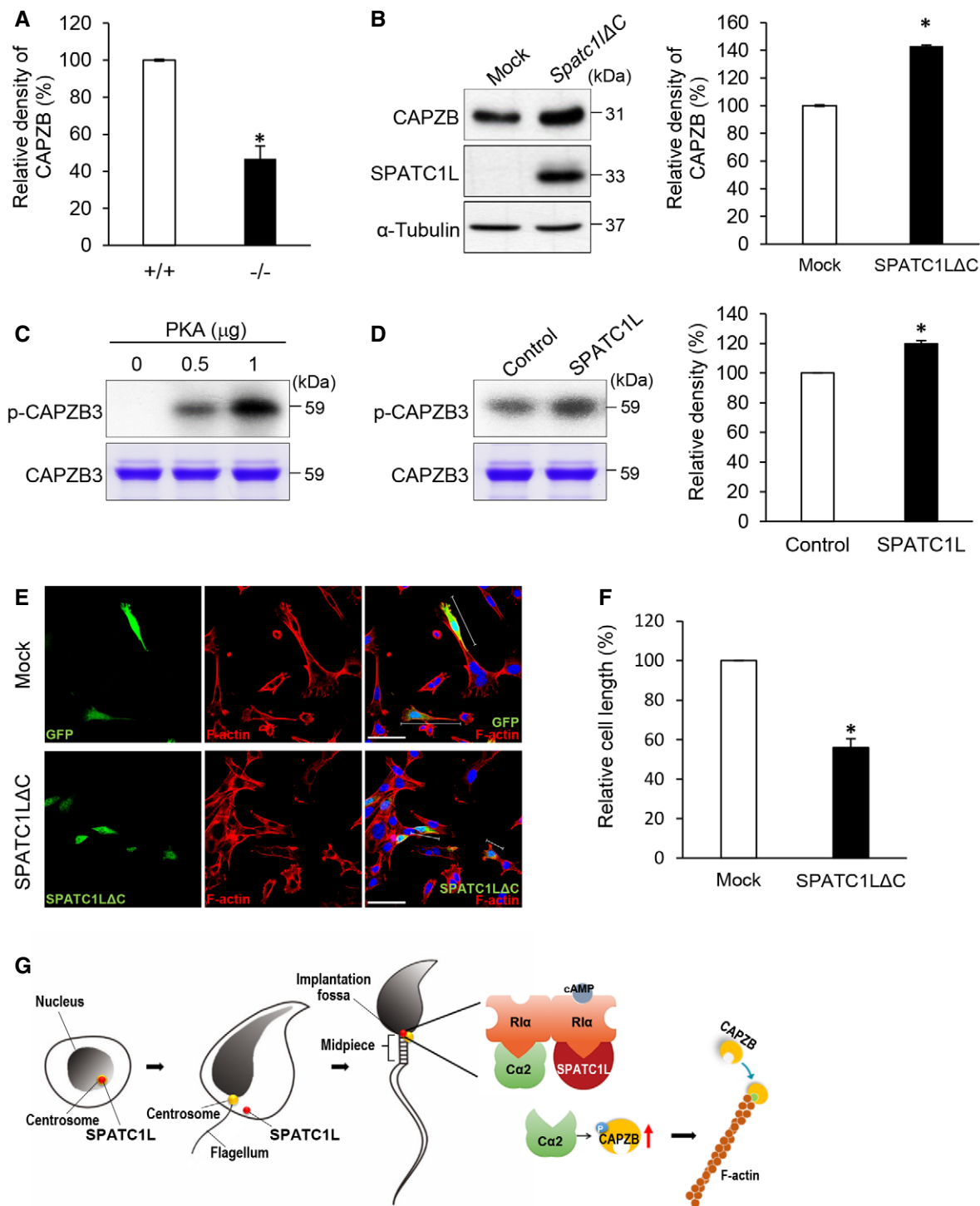


Figure 8.

We further found that SPATC1L is associated with the PKA complex. PKA is an ubiquitous serine/threonine protein kinase present in all eukaryotes that has been demonstrated to regulate diverse processes, including growth, metabolism, gene expression, development, and memory [20]. PKA forms an inactive holoenzyme containing a regulatory subunit dimer and two catalytic subunits.

During spermatogenesis, expression of PKA subunits is tightly regulated at each stage [21]. In male germ cells, an alternative promoter present in the first intron of the *Cα* gene becomes transcriptionally active, switching expression from the *Cα1* to the *Cα2* isoform during the pachytene stage of spermatogenesis [19,29,30]. However, the roles of PKA in spermatogenic cell centrosomes and flagellar basal

bodies during sperm development have not been elucidated, despite the fact that PKA is known for its roles in sperm capacitation [21]. We found that SPATC1L increases PKA activity, potentially through binding to the R subunit. It is well known that PKA is activated by cAMP binding to the R subunit. Although we do not know how the involvement of SPATC1L in PKA activity is related to cAMP, our study provides the first remarkable finding that PKA can be regulated by this germ cell-specific protein in addition to cAMP.

Using *Spatc1l*-KO mice, we found that KO male mice were sterile owing to acephalic spermatozoa. We further found that the amount of SPATC1L protein is important for the stability of the head-tail junction, because heterozygous (*Spatc1l*<sup>+/-</sup>) male mice with a reduction in the amount of SPATC1L exhibited subfertility, showing haploinsufficiency. Indeed, we had difficulty in obtaining homozygous KO mice because of the subfertility of *Spatc1l*<sup>+/-</sup> males. The CRISPR/Cas9 genome editing method is advantageous in this context, because we were able to observe the phenotype of KO mice using founder mice with a bi-allele deletion. Acephaly in sperm, an abnormality that represents a type of teratozoospermia, is associated with some of the male infertility cases [12] and has been linked to loss of function of several genes [31–36]. They include genes encoding protease serine 21 (PRSS21), ornithine decarboxylase anti-enzyme 3 (OAZ3), outer dense fiber 1 (ODF1), Sad1 and UNC84 domain containing 5 (SUN5), and spermatogenesis associated 6 (SPATA6). In particular, SPATA6 was found to function in the structural formation of the sperm neck components. Despite the importance of these proteins in the head-tail linkage, the direct molecular regulatory mechanisms involved in maintaining the integrity of the sperm head-tail junction remain unclear. Our study provides key information on the potential role of SPATC1L in stabilizing the sperm head-tail attachment during spermiogenesis. In mammalian sperm, the flagellum is attached to the base of the head by the connecting piece. This structure is composed of the segmented column, basal plate, and capitulum [37]. Our finding that structures in the connecting piece in *Spatc1l*-KO testicular sperm are normal suggests that SPATC1L is not involved in the structural development of the connecting piece. Indeed, head-tail separation of KO sperm occurred between the basal plate and capitulum in the implantation fossa. Given our findings regarding the localization and interacting partners of SPATC1L, the maintenance of PKA activity by SPATC1L in the implantation fossa may be essential for stabilizing this region. We often observed sperm in which a detached head was dislocated to the midpiece inside the same plasma membrane surrounding the sperm strongly suggests that disengagement of sperm heads from tails does not reflect structural destruction involving a physical force, but rather indicates instability of the implantation fossa.

It has been reported that genetic mutations in mice that affect PKA signaling in germ cells lead to infertility. In humans, nearly two-thirds of Carney complex patients, with a haploinsufficiency of *RI $\alpha$* , have significantly reduced fertility owing to sperm morphology defects and azoospermia or oligospermia [38–41]. However, PKA activity has only been studied in the context of sperm capacitation and motility that are directly required for fertilization. In this study, we provide the first identification of CAPZB, a protein that forms a heterodimer with CAPZA mediates calcium-independent capping of fast-growing (barbed) ends of actin filaments and thereby protects actin filaments from assembly and disassembly [42–44], as a target of PKA phosphorylation in the implantation fossa. We show for the

first time that CAPZB can be phosphorylated by PKA, and the levels of the phosphorylation and amount of CAPZB are increased by SPATC1L. Moreover, the length of F-actin was decreased by SPATC1L in cultured cells, implying that activity of CAPZB is promoted by SPATC1L. F-actin has been suggested to play a role in shaping the acrosome, attaching the acrosome to the spermatid nucleus, and removing cytoplasm during spermiation [45–49]. Despite the presence of F-actin in the neck region of sperm, the roles of F-actin in this region during spermiogenesis have not yet been studied [50]. In the subacrosomal region, F-actin is expected to function in anchoring of the inner acrosomal membrane and stabilization of the acrosome to the nuclear envelope on the spermatid head [48]. Thus, it is possible that F-actin also functions in stabilizing head-tail attachment in the neck region of sperm. In this process, F-actin polymerization can be regulated and stabilized by CAPZB that has been phosphorylated (activated) by SPATC1L-activated PKA in the implantation fossa. Further studies are necessary to establish whether F-actin attaches the basal plate at the caudal pole of the nucleus to the capitulum in the connecting piece.

In summary, we have discovered that the novel germ cell-specific protein SPATC1L is involved in the maintenance of sperm head-tail attachment during spermiogenesis, possibly via a PKA regulatory mechanism in which phosphorylated CAPZB acts as a mediator. Previous studies have reported decapitated and decaudated spermatozoa in several patients with infertility of genetic origin [12,51]. Our findings may offer insight into the mechanism of spermiogenesis and will help in the investigation of causes of human infertility.

## Materials and Methods

### Ethics statement

The human testicular biospecimens used in this study were provided by the Pusan National University Hospital; this hospital is a member of the National Biobank of Korea, which is supported by the Ministry of Health, Welfare and Family Affairs. All samples from the National Biobank of Korea were obtained with informed consent under institutional review board-approved protocols. The study of human sperm was also ratified through the Ethics Committee of Gwangju Institute of Science and Technology (GIST) and Chonnam National University (permit number: 20140818-BR-14-01-02). All participants signed an informed consent form permitting use of their semen remnants in this study. All animal experiments were performed in accordance with Korean Food and Drug Administration (KFDA) guidelines. Protocols were reviewed and approved by the Institutional Animal Care and Use Committees (IACUC) of MacroGen, Inc. and GIST (permit number: GIST 2011-13).

### Antibodies

Polyclonal antisera against mouse SPATC1L were produced in a previous study from rabbits immunized with the antigen, GST-SPATC1L (amino acid region 101–200). The antibody was affinity-purified using the corresponding protein and an AminoLink Immobilization kit (Thermo Scientific Pierce Protein Research, Waltham,

MA, USA). The resulting purified anti-SPATC1L antibody was used for immunoblot (4 µg/ml) and immunofluorescence (7 µg/ml) analyses. Immunoblot analyses also used monoclonal anti-mouse ADAM2 (1:1,000, Millipore, Billerica, MA), anti-His (1:1,000, Amersham, Arlington Heights, IL USA), anti- $\alpha$ -tubulin (1:1,000, Millipore), and polyclonal anti-GAPDH (1:1,000, Ab Frontier, Seoul, South Korea), anti-GST (1:1,000, Amersham), anti-RI $\alpha$  (1:1,000, BD Biosciences, NJ, USA; Abcam, Cambridge, MA), and anti-PRKACA (C $\alpha$ ; 1:500, Abcam, Cambridge, MA) antibodies. Immunofluorescence analyses used anti-RI $\alpha$  (GeneTex, Cambridge, MA) and anti-AKAP11 primary antibodies (1:100, Santa Cruz, Dallas, TX USA), anti- $\gamma$ -tubulin antibodies (1:5,000, Sigma, Oakville, Canada, ON), and rhodamine-conjugated anti-rabbit (red; 1:100, Molecular Probes, Eugene, OR USA) or Alexa Fluor 488-conjugated anti-mouse (green; 1:100, Jackson ImmunoResearch, West Grove, PA) secondary antibodies; the nucleic acid dye Hoechst 33342 (1:1,000, Thermo Fisher, Waltham, MA) was used to stain nuclei. For immunoblot analyses of the five candidate proteins identified by 2DE-PMF, we used anti-EFHD2 (0.5 µg/ml; Novus, Littleton, CO), anti-SRSF1 (0.5 µg/ml; Thermo), anti-CAPZB (1:1,000; Abcam), anti-SERPINB6A (1:500; Novus), and anti-ERLIN2 (1:200; Sigma) primary antibodies.

#### Preparation of testicular cells, testicular sperm, and mature sperm

Cells were isolated from mice in Mg<sup>2+</sup>-HEPES buffer. Testicular germ cells and testicular sperm were separated by 52% (v/v) gradient of isotonic Percoll (GE Healthcare) and centrifuged for 10 min (27,000 × g, 4°C), and the isolated cells were resuspended with Mg<sup>2+</sup>-HEPES buffer. Mature sperm were prepared from the cauda epididymides and vas deferens.

#### Protein samples and immunoblot analysis

Immunoblot analyses were performed using protein samples obtained from the testes of adult male mice (8 weeks) or male mice of different ages. Protein samples were prepared in 1% sodium dodecyl sulfate (SDS) lysis buffer containing a protease inhibitor cocktail and were denatured by boiling for 10 min in the presence of 3% SDS and 5%  $\beta$ -mercaptoethanol (2× sample buffer). Each sample containing ~100 µg of protein was separated by SDS-PAGE and transferred to polyvinylidene difluoride membranes (Bio-Rad, Mississauga, ON, Canada). Membranes were blocked in 5% nonfat dry milk and incubated with primary antibodies for 3 h. For competition assay, primary antibody was preliminarily incubated with 1 mg of antigen (GST or GST-SPATC1L) for 6 h at 4°C. Testicular cells and testicular sperm were isolated from testes of adult male mice by suspending in 52% isotonic Percoll (GE Healthcare, Pittsburgh, PA) followed by centrifugation for 30 min (38,512 g, 4°C) [52]. Mature sperm from the cauda epididymis and vas deferens were directly released into phosphate-buffered saline (PBS).

#### Immunofluorescence and immunohistochemistry

Isolated testicular cells, testicular sperm, and epididymal sperm were fixed in 4% paraformaldehyde for 30 min at room

temperature and permeabilized in 0.5% Triton X-100 for 10 min at room temperature. For visualization of the centrosome, cells were treated with ice-cold methanol for 2 min at -20°C. After blocking with 3% bovine serum albumin for 30 min, samples were incubated first with primary antibodies for 2 h at room temperature, and then with rhodamine- and/or Alexa Fluor 488-conjugated secondary antibodies, diluted 1:1,000. Fluorescence signals were observed under a confocal microscope (FLUOVIEW FV1000, Olympus, Shinjuku, Japan). Paraffin section blocks were prepared by fixing testes obtained from adult mice with Bouin solution (Sigma) overnight at room temperature, and then dehydrating the tissue with a graded series of 70, 80, 90, 95 and 100% ethanol. Testes were incubated in a mixture of xylene and ethanol (1:1), followed by 100% xylene at room temperature for 1 h, and then incubated sequentially in a mixture of xylene and paraffin (1:1) at 70°C for 1 h and 100% paraffin at 70°C overnight. Finally, testes were embedded in paraffin and dried overnight. After heating in a microwave oven for 20 min, paraffin-embedded sections of mouse testes were deparaffinized using xylene and rehydrated with a graded series of 100, 90, 80 and 70% ethanol and tap water. Sections were stained with hematoxylin (Sigma) for 3 min, washed, and then stained with eosin Y (Sigma) for 1 min. After dehydration with a graded series of 70, 80, 90, 95 and 100% ethanol and 100% xylene, stained sections were observed under an Aperio Scanscope (Leica Microsystems, Germany).

#### Immunoprecipitation

Testes or cells were lysed in nonionic detergent buffer (1% Nonidet P-40, 150 mM sodium chloride, 50 mM Tris-Cl, 1 mM EDTA) containing protease inhibitor cocktail. Total tissue lysates (1 mg) or total cell lysates (500 µg) were incubated with 5 µg of anti-SPATC1L or anti-GST antibody, or normal rabbit serum, together with protein A-Sepharose (Amersham Biosciences) at 4°C overnight. After washing the beads three times with lysis buffer, bound proteins were eluted with 8 M urea (proteomic analysis) or boiled for 10 min with 3% SDS sample buffer (immunoblot analysis).

#### Capillary reverse-phase liquid chromatography (LC)-tandem mass spectrometry (MS/MS) and data analysis

Trypsin-digested proteins were loaded onto fused silica capillary columns (100 µm i.d., 360 µm o.d.) containing 7.5 cm of 5 µm particle Aqua C18 reversed-phase column material (Phenomenex, Torrance, CA USA), placed in line with an Agilent HP1100 quaternary LC pump. The flow rate was 250 nl/min, achieved using a splitter system. Peptides were eluted with a gradient of buffer A (5% acetonitrile and 0.1% formic acid) and buffer B (80% acetonitrile and 0.1% formic acid) starting with 100% buffer A for 3 min, followed by 0–15% buffer B for 5 min, 15–55% buffer B for 57 min, and 55–100% buffer B for 15 min (total run time, 80 min). Eluted peptides were directly electrosprayed into an LTQ Ion Trap mass spectrometer (ThermoFinnigan, Palo Alto, CA) by applying a DC voltage of 2.3 kV. A data-dependent scan consisting of one full MS scan (400–2,000 *m/z*) and ten data-dependent MS/MS scans was used to generate MS/MS spectra of eluted peptides. A normalized collision energy of 35% was used throughout the data-acquisition period. MS/MS spectra were compared with the Mouse IPI protein

database (ver.3.31) using TurboSEQUENT and SEQUEST Cluster Systems (14 nodes). DTASelect was used to filter the search results, and Xcorr values were applied to different charge states of peptides, with a fully trypsin-digested end requirement of 1.8 for singly charged peptides, 2.2 for doubly charged peptides, and 3.2 for triply charged peptides; a delta Cn value of 0.08 was applied to all charge states. Protein database search results were confirmed by a subsequent manual assignment of fragment ions in all filtered MS/MS spectra.

### **In vitro binding assay**

For *in vitro* binding assays, full-length SPATC1L was amplified from mouse testis cDNA by polymerase chain reaction (PCR) using the primers 5'-AAG GAT CCA TAT GGC AGA GGG TAG CG-3' (forward) and 5'-CGG AAT TCG TCA CCA GGC AAA GAG T-3' (reverse) incorporating 5' *Bam*HI and 3' *Eco*RI sites, and cloned into the pGEX-5x-2 vector. Full-length RI $\alpha$  and regions 1–6 were amplified from mouse testis cDNA using the following primer pairs: full length, 5'-TGG ATC CG A TGG CGT CTG GCA GTA TG-3' (forward) and 5'-AGC GGC CGC GAC GGA CAG GGA CAC GAA-3' (reverse); region 1, 5'-TGG ATC CG A TGG CGT CTG GCA GTA TG-3' (forward) and 5'-AGC GGC CGC CAC ATT CTT TTC GAT GG-3' (reverse); region 2, 5'-TGG ATC CGC TGT TTT CAC ACC TTG ATG A-3' (forward) and 5'-AGC GGC CGC CAC TTT ACT AAG GAA TTC TT-3' (reverse); region 3, 5'-CCG GAT CCG ATT TTA GAG TCT CTG GAC AAG-3' (forward) and 5'-AGC GGC CGC GAC GGA CAG GGA CAC GAA-3' (reverse); for regions 4–6, we used a combination of the primers described above. The resulting PCR products were cloned into the pET-28b vector and expressed in the *Escherichia coli* BL21 strain. Glutathione-S-transferase (GST)-fused SPATC1L protein and His-fused RI $\alpha$  proteins were affinity-purified using glutathione-Sepharose 4B (GE Healthcare) and Ni-Sepharose 6 Fast Flow (Amersham) affinity chromatography, respectively. Binding reactions were performed by incubating 150 nM purified GST-SPATC1L or GST only (control) with 90 nM His-RI $\alpha$  protein together with 5  $\mu$ g of anti-SPATC1L or anti-GST antibody bound to protein A-Sepharose beads in binding buffer (PBS, 5% nonfat dry milk) at 4°C for 3 h. After washing three times, beads were boiled for 10 min with 3% SDS sample buffer for immunoblot analyses.

### **Cell culture and PKA activity assay**

TM4 cells were obtained from the American Type Culture Collection (ATCC no. CRL-1715; ATCC) and cultured at 5% CO<sub>2</sub> in Dulbecco's modified Eagle's medium F12 (Invitrogen, Burlington, ON, Canada) supplemented with 5% horse serum and 2.5% fetal bovine serum at 37°C. For PKA activity assays, full-length SPATC1L was amplified from mouse testis cDNA using the primers, 5'-AAG GAT CCA TGG CAG AGG GTA GCG AA-3' (forward) and 5'-CGG AAT TCG CCA GGC AAA GAG TG-3' (reverse) incorporating 5' *Bam*HI and 3' *Eco*RI sites, and cloned into the pcDNA3.1B vector. Cells were transiently transfected with the pcDNA3.1B vector construct using Lipofectamine LTX (Invitrogen), according to the manufacturer's instructions. Cells were treated with or without dbcAMP (500  $\mu$ M) during transfection. Twenty-four hours after transfection, cells were lysed in lysis buffer (1% Nonidet P-40, 20 mM MOPS, 5 mM EGTA, 1 mM phenylmethanesulfonyl fluoride, 1 mM benzamide)

containing protease and phosphatase inhibitor cocktails at 4°C for 30 min. After centrifugation, 0.2  $\mu$ g of cleared supernatant (cytosolic fraction) was used for PKA activity assays; cells transfected with pcDNA3.1B vector only were used as negative controls. Isolated testicular sperm were also lysed as described above, and 1  $\mu$ g of lysate was used for PKA activity assays. The assay was performed using a PKA kinase activity kit (Enzo Life Sciences, Arlington Heights, IL USA) according to the manufacturer's instructions. Absorbance was measured at a wavelength of 450 nm, and relative kinase activity was calculated using the formula, Relative activity = (average absorbance<sub>(sample)</sub> – average absorbance<sub>(blank)</sub>)/quantity of crude protein used per assay. Assays were performed more than 10 times, and the PKA activity of each sample was measured in triplicate wells.

### **Cilia length measurement**

TM4 cells were transiently transfected with the pcDNA3.1B vector construct. Twenty-four hours after transfection, the cells were incubated in serum starved medium (serum-free DMEM/F12) for 24 h to induce ciliogenesis. The cells were then fixed and permeabilized. To visualize cilia with centrosome, co-immunostaining was performed using anti-acetyl- $\alpha$ -tubulin antibody (red; 0.05  $\mu$ g/ml, Sigma) for cilia and anti- $\gamma$ -tubulin antibody (yellow; 1:5,000, Sigma) for centrosome. Cilia lengths were measured by ImageJ.

### **Generation of Spatc1l-KO mice**

*Spact1l*-KO mice were generated by MacroGen, Inc. (Seoul, Korea) using Cas9 protein tagged with a nuclear localization signal and gRNAs targeting exon 1 of the *Spact1l* gene (ToolGen Inc., Seoul, South Korea). Briefly, C57BL/6N female mice were treated with pregnant mare's serum gonadotropin (PMSG) and human chorionic gonadotropin (HCG), and mated 48 h later with C57BL/6N male mice. The next day, female mice were checked for the presence of a vaginal plug, after which they were sacrificed and their fertilized embryos were harvested. The activities of gRNAs designed to knock out the *Spact1l* gene (1, 5'-TGG TGT CAG GTA CTC ACA CAT GG-3'; 2, 5'-CAG TTC GCT ACC CTC TGC CAT GG-3'; 3, 5'-GAG CTG TGG TCG AGG GAG CCG GG-3'; and 4, 5'-TCA GGG TAG GTA GGG ACC TTG GG-3') were validated using *in vitro* cleavage reactions. In these reactions, the amplified *Spact1l* gene, used as a template, was incubated with 20 nM Cas9 protein and 40 nM sgRNA in 1 $\times$  NEB 3 buffer for 90 min at 37°C, and then, reactions were stopped by adding stop solution (30% glycerol, 1.2% SDS, 100 mM EDTA). After confirming cleavage activity by electrophoresis of reaction mixtures, one-cell embryos were microinjected with sgRNA and Cas9 protein mixture and incubated at 37°C for 1–2 h. Fourteen to sixteen injected one-cell-stage embryos were transplanted into the oviducts of pseudopregnant recipient mice (ICR). After F0 mice were born, tail snips were collected for genotyping, performed by PCR using the primer pair, 5'-GCC GCC TCT TTA AGG GTA AC-3' (forward) and 5'-CTA AGC CTG CAC CTC ACC TC-3' (reverse), followed by assay with mismatch-sensitive T7 endonuclease, T7E1 (M0302S; New England Biolabs, MA). TA cloning was performed on T7E1-positive samples followed by sequence analysis. For genotyping of completed KO mice, PCR was performed using the primer pair 5'-GAG GAG CAG ATG AGG AAG AAG GAC GTT-3' (forward) and



5'-TGG AGC CCT GGA ATC ACA CCC TGC-3' (reverse). The resulting *Spatc1l*-KO mice were interbred and maintained under pathogen-free conditions at Macrogen, Inc.

### Phenotypic analyses of *Spatc1l*-KO mice

For fertility tests of male mice, each *Spatc1l*-KO and WT male (8 weeks old) was placed with two C57BL/6 females. The females were checked for the presence of vaginal plugs, indicating pregnancy. After dams had delivered, the number of pups was counted, and the fertility rate was calculated. For sperm counts, sperm from the cauda epididymis and vas deferens from 8-week-old *Spatc1l*-KO and WT male mice were collected and counted in a hemocytometer under a light microscope. Testis and epididymis weights were measured and expressed relative to total body weight.

### SEM and TEM analyses

Sperm obtained from the vas deferens were fixed in Karnovsky fixative (0.2 M cacodylate buffer, 3% paraformaldehyde, 3% glutaraldehyde, 0.2% picric acid) for 4 h at 4°C, washed three times with 0.1 M PBS, then post-fixed with 1% OsO<sub>4</sub> in 0.1 M cacodylate buffer for 2 h at 4°C. After washing with 0.1 M PBS, the specimens were dehydrated with a graded series of 70, 80, 90, 95 and 100% ethanol. Sperm samples were then coated in a low vacuum and observed under a Hitachi S-4700 scanning electron microscope at 10 kV. For TEM analyses, the testis obtained from an adult mouse was fixed in Karnovsky fixative as described above. In this case, after dehydration, the specimens were incubated in propylene oxide followed by embedding in a mixture of Epon 812 and Araldite (Polysciences Inc., Warrington, PA). Ultrathin sections (70 nm) were cut using an Em UC6 Ultramicrotome (Leica). The sections were collected on TEM nickel grids and observed using a transmission electron microscope (Tecnai G2; FEI Company Inc., Hillsboro, OR) at 120 kV.

### 2DE-PMF analysis

Testes obtained from an adult WT or *Spatc1l*-KO mouse were homogenized directly in lysis buffer (7 M urea, 2 M thiourea containing 4% CHAPS, 1% dithiothreitol [DTT], 2% pharmalyte, and 1 mM benzamide) using a motor-driven homogenizer (PowerGen125). Proteins were extracted for 1 h at room temperature with vortexing and then centrifuged. For the first dimension of 2DE, a sample of the soluble fraction containing 200 µg protein was loaded onto the gel, followed by isoelectric focusing (IEF) at 20°C using a Multiphor II electrophoresis unit and EPS 3500 XL power supply (Amersham). For IEF, the voltage was linearly increased from 150 to 3,500 V for 3 h during sample entry, followed by a constant 3,500 V; focusing was complete after 96 kWh. Prior to resolving in the second dimension, strips were incubated for 10 min in equilibration buffer (50 mM Tris-Cl, 6 M urea, 2% SDS, and 30% glycerol), followed by 1% DTT and then 2.5% iodoacetamide. Equilibrated strips were inserted onto 10–16% gradient SDS-PAGE gels (20 × 24 cm) and electrophoresed using a Hoefer DALT 2D system (Amersham). Gels were stained with colloidal Coomassie Brilliant Blue for all proteins and with ProQ Diamond (Invitrogen) for phosphoproteins, following the manufacturer's instructions. Digitized images were quantitatively analyzed

using PDQuest software (version 7.0; Bio-Rad) according to the protocols provided by the manufacturer. The quantity of each spot was normalized to the total intensity of valid spots. Protein spots were selected based on a significant, ≥ 2-fold difference in phosphorylation level compared with the WT sample. Protein spots, identified by PMF, were excised, digested with trypsin (Promega, Madison, WI USA), mixed with α-cyano-4-hydroxycinnamic acid in 50% acetonitrile/0.1% TFA, and subjected to MALDI-TOF analysis (Microflex LRF 20; Bruker Daltonics, Billerica, MA USA). Spectra were collected from 300 shots per spectrum over the *m/z* range 600–3,000 and calibrated by two-point internal calibration using trypsin auto-digestion peaks (*m/z* 842.5099, 2211.1046). The peak list was generated using Flex Analysis 3.0. The threshold used for peak selection was 500 for minimum resolution of monoisotopic mass, and a signal-to-noise ratio (S/N) of 5 or greater. The search program MASCOT, developed by Matrix Science (<http://www.matrixscience.com/>), was used for protein identification by PMF.

### In vitro kinase assay

Full-length SPATC1L was amplified as described above, and full-length CAPZB3 was amplified from mouse testis cDNA by polymerase chain reaction (PCR) using the primers 5'-TGG AAT TCC TAT GCA TCC TAG CAG GC-3' (forward) and 5'-ACT CGA GTC AAC ACT GCT GCT TTC TC-3' (reverse) incorporating 5' *EcoRI* and 3' *XhoI* sites, and cloned into the pGEX-5x-2 vector and expressed in the *Escherichia coli* BL21 strain. GST-fused CAPZB3 protein was affinity-purified using glutathione-Sepharose 4B (GE Healthcare) affinity chromatography. Kinase reaction was performed in kinase reaction buffer supplemented with 10 µg of GST-CAPZB3 or 10 µg of BPDEtide (Enzo Life Sciences) as a substrate, and 500 ng of PKA holoenzyme (Sigma, Oakville, Canada, ON). The reactions were initiated by addition of 0.2 mM ATP/Mg<sup>2+</sup> (Sigma-Aldrich) and 10 µM cAMP containing 10 µCi of (γ-<sup>32</sup>P) ATP (3,000 Ci/mmol/l, Perkin-Elmer, Waltham, MA, USA). For *in vitro* kinase assay with SPATC1L, 10 ng of GST-SPATC1L or GST only (control) was added to kinase reaction buffer. The mixture was incubated for 1 h at 30°C, and the reaction was stopped by boiling in SDS sample buffer containing 5% (v/v) β-mercaptoethanol. The kinase reaction was visualized by autoradiography of SDS-PAGE gel.

### Statistics

Results are presented as means ± standard deviation (SD) values. The statistical significance of differences between data means was determined using a two-tailed Student's *t*-test. Each experiment was performed at least three times to obtain minimum number for SD.

**Expanded View** for this article is available online.

### Acknowledgements

This work was supported by Mid-career Researcher Program through National Research Foundation of Korea funded by the Ministry of Science, ICT & Future Planning (NRF-2015R1A2A2A01005300), the Bio & Medical Technology Development Program of the National Research Foundation of Korea funded by the Ministry of Science, ICT & Future Planning (NRF 2013M3A9A7046297) and GIST Research Institute (GRI), Korea.

## Author contributions

JihK, EME, and CC conceived the study. JihK and CC designed the experiments; JihK performed the experiments; jihk, EME, and CC analyzed the data; KHC performed electron microscopy; JTK, Jj, JaK, SHH, JiK, and ZYP contributed reagents/materials/analysis tools; jihK and CC wrote the paper.

## Conflict of interest

The authors declare that they have no conflict of interest.

## References

- Eddy EM (1995) "Chauvinist genes" of male germ cells: gene expression during mouse spermatogenesis. *Reprod Fertil Dev* 7: 695–704
- Eddy EM (1998) Regulation of gene expression during spermatogenesis. *Semin Cell Dev Biol* 9: 451–457
- Eddy EM (2002) Male germ cell gene expression. *Recent Prog Horm Res* 57: 103–128
- Skakkebaek NE, Jorgensen N, Main KM, Rajpert-De Meyts E, Leffers H, Andersson AM, Juul A, Carlsen E, Mortensen GK, Jensen TK et al (2006) Is human fecundity declining? *Int J Androl* 29: 2–11
- Hong S, Choi I, Woo JM, Oh J, Kim T, Choi E, Kim TW, Jung YK, Kim DH, Sun CH et al (2005) Identification and integrative analysis of 28 novel genes specifically expressed and developmentally regulated in murine spermatogenic cells. *J Biol Chem* 280: 7685–7693
- Fry RC, Svensson JP, Valiathan C, Wang E, Hogan BJ, Bhattacharya S, Bugni JM, Whittaker CA, Samson LD (2008) Genomic predictors of interindividual differences in response to DNA damaging agents. *Genes Dev* 22: 2621–2626
- Bellve AR, Millette CF, Bhatnagar YM, O'Brien DA (1977) Dissociation of the mouse testis and characterization of isolated spermatogenic cells. *J Histochem Cytochem* 25: 480–494
- Baek N, Woo JM, Han C, Choi E, Park I, Kim DH, Eddy EM, Cho C (2008) Characterization of eight novel proteins with male germ cell-specific expression in mouse. *Reprod Biol Endocrinol* 6: 32
- Le Lannou D (1979) [Teratospermia consisting of the absence of the head of the spermatozoa because of a fault in the joint between the head and the neck of the sperm in man (author's transl)]. *J Gynecol Obstet Biol Reprod* 8: 43–45
- Chemes HE, Carizza C, Scarinci F, Brugo S, Neuspiller N, Schwarsztein L (1987) Lack of a head in human spermatozoa from sterile patients: a syndrome associated with impaired fertilization. *Fertil Steril* 47: 310–316
- Panidis D, Matalliotakis I, Rousso D, Mavromatidis G, Koumantakis E, Mamopoulos M (1998) Headless spermatozoa in fertile men. *J Obstet Gynaecol* 18: 581–583
- Chemes HE, Puigdomenech ET, Carizza C, Olmedo SB, Zanchetti F, Hermes R (1999) Acephalic spermatozoa and abnormal development of the head-neck attachment: a human syndrome of genetic origin. *Hum Reprod* 14: 1811–1818
- Kamal A, Mansour R, Fahmy I, Serour G, Rhodes C, Aboulghar M (1999) Easily decapitated spermatozoa defect: a possible cause of unexplained infertility. *Hum Reprod* 14: 2791–2795
- Panidis D, Rousso D, Kourtis A, Gianoulis C, Papatheanasiou K, Kalachanis J (2001) Headless spermatozoa in semen specimens from fertile and subfertile men. *J Reprod Med* 46: 947–950
- Rawe VY, Terada Y, Nakamura S, Chillik CF, Olmedo SB, Chemes HE (2002) A pathology of the sperm centriole responsible for defective sperm aster formation, syngamy and cleavage. *Hum Reprod* 17: 2344–2349
- Chemes HE, Rawe VY (2010) The making of abnormal spermatozoa: cellular and molecular mechanisms underlying pathological spermiogenesis. *Cell Tissue Res* 341: 349–357
- Reinton N, Collas P, Haugen TB, Skalhegg BS, Hansson V, Jahnsen T, Tasken K (2000) Localization of a novel human A-kinase-anchoring protein, hAKAP220, during spermatogenesis. *Dev Biol* 223: 194–204
- Pidoux G, Tasken K (2010) Specificity and spatial dynamics of protein kinase A signaling organized by A-kinase-anchoring proteins. *J Mol Endocrinol* 44: 271–284
- Desseyn JL, Burton KA, McKnight GS (2000) Expression of a nonmyristylated variant of the catalytic subunit of protein kinase A during male germ-cell development. *Proc Natl Acad Sci USA* 97: 6433–6438
- Skalhegg BS, Tasken K (2000) Specificity in the cAMP/PKA signaling pathway. Differential expression, regulation, and subcellular localization of subunits of PKA. *Front Biosci* 5: D678–D693
- Burton KA, McKnight GS (2007) PKA, germ cells, and fertility. *Physiology* 22: 40–46
- Kim C, Cheng CY, Saldanha SA, Taylor SS (2007) PKA-I holoenzyme structure reveals a mechanism for cAMP-dependent activation. *Cell* 130: 1032–1043
- Wisniewski JR, Nagaraj N, Zougman A, Gnäd F, Mann M (2010) Brain phosphoproteome obtained by a FASP-based method reveals plasma membrane protein topology. *J Proteome Res* 9: 3280–3289
- Mertins P, Yang F, Liu T, Mani DR, Petyuk VA, Gillette MA, Clauser KR, Qiao JW, Gritsenko MA, Moore RJ et al (2014) Ischemia in tumors induces early and sustained phosphorylation changes in stress kinase pathways but does not affect global protein levels. *Mol Cell Proteomics* 13: 1690–1704
- Paavilainen VO, Bertling E, Falck S, Lappalainen P (2004) Regulation of cytoskeletal dynamics by actin-monomer-binding proteins. *Trends Cell Biol* 14: 386–394
- Narita A, Takeda S, Yamashita A, Maeda Y (2006) Structural basis of actin filament capping at the barbed-end: a cryo-electron microscopy study. *EMBO J* 25: 5626–5633
- Goto M, Eddy EM (2004) Speriolin is a novel spermatogenic cell-specific centrosomal protein associated with the seventh WD motif of Cdc20. *J Biol Chem* 279: 42128–42138
- Goto M, O'Brien DA, Eddy EM (2010) Speriolin is a novel human and mouse sperm centrosome protein. *Hum Reprod* 25: 1884–1894
- San Agustín JT, Witman GB (2001) Differential expression of the C(s) and Calpha1 isoforms of the catalytic subunit of cyclic 3',5'-adenosine monophosphate-dependent protein kinase testicular cells. *Biol Reprod* 65: 151–164
- Vetter MM, Zenn HM, Mendez E, van den Boom H, Herberg FW, Skalhegg BS (2011) The testis-specific Calpha2 subunit of PKA is kinetically indistinguishable from the common Calpha1 subunit of PKA. *BMC Biochem* 12: 40
- Netzel-Arnett S, Bugge TH, Hess RA, Carnes K, Stringer BW, Scarman AL, Hooper JD, Tonks ID, Kay GF, Antalis TM (2009) The glycosylphosphatidylinositol-anchored serine protease PRSS21 (testisin) imparts murine epididymal sperm cell maturation and fertilizing ability. *Biol Reprod* 81: 921–932
- Tokuhiro K, Isotani A, Yokota S, Yano Y, Oshio S, Hirose M, Wada M, Fujita K, Ogawa Y, Okabe M et al (2009) OAZ-t/OAZ3 is essential for rigid connection of sperm tails to heads in mouse. *PLoS Genet* 5: e1000712

33. Yang K, Meinhardt A, Zhang B, Grzmil P, Adham IM, Hoyer-Fender S (2012) The small heat shock protein ODF1/HSPB10 is essential for tight linkage of sperm head to tail and male fertility in mice. *Mol Cell Biol* 32: 216–225
34. Yang K, Grzmil P, Meinhardt A, Hoyer-Fender S (2014) Haplo-deficiency of ODF1/HSPB10 in mouse sperm causes relaxation of head-to-tail linkage. *Reproduction* 148: 499–506
35. Yuan S, Stratton CJ, Bao J, Zheng H, Bhetwal BP, Yanagimachi R, Yan W (2015) Spata6 is required for normal assembly of the sperm connecting piece and tight head-tail conjunction. *Proc Natl Acad Sci USA* 112: E430–E439
36. Zhu F, Wang F, Yang X, Zhang J, Wu H, Zhang Z, Zhang Z, He X, Zhou P, Wei Z et al (2016) Biallelic SUN5 mutations cause autosomal-recessive acephalic spermatozoa syndrome. *Am J Hum Genet* 99: 1405
37. Hamasaki M, Wakimoto M, Maehara T, Matsuo H (1994) Three-dimensional structures of the neck region of the hamster spermatozoa in the caudal epididymis. *Arch Histol Cytol* 57: 59–65
38. Stratakis CA (2002) Mutations of the gene encoding the protein kinase A type I-alpha regulatory subunit (PRKAR1A) in patients with the “complex of spotty skin pigmentation, myxomas, endocrine overactivity, and schwannomas” (Carney complex). *Ann N Y Acad Sci* 968: 3–21
39. Nolan MA, Babcock DF, Wennemuth G, Brown W, Burton KA, McKnight GS (2004) Sperm-specific protein kinase A catalytic subunit Calpha2 orchestrates cAMP signaling for male fertility. *Proc Natl Acad Sci USA* 101: 13483–13488
40. Veugelers M, Wilkes D, Burton K, McDermott DA, Song Y, Goldstein MM, La Perle K, Vaughan CJ, O'Hagan A, Bennett KR et al (2004) Comparative PRKAR1A genotype-phenotype analyses in humans with Carney complex and prkar1a haploinsufficient mice. *Proc Natl Acad Sci USA* 101: 14222–14227
41. Burton KA, McDermott DA, Wilkes D, Poulsen MN, Nolan MA, Goldstein M, Basson CT, McKnight GS (2006) Haploinsufficiency at the protein kinase A RI alpha gene locus leads to fertility defects in male mice and men. *Mol Endocrinol* 20: 2504–2513
42. Nachmias VT, Golla R, Casella JF, Barron-Casella E (1996) Cap Z, a calcium insensitive capping protein in resting and activated platelets. *FEBS Lett* 378: 258–262
43. Wear MA, Cooper JA (2004) Capping protein: new insights into mechanism and regulation. *Trends Biochem Sci* 29: 418–428
44. Cooper JA, Sept D (2008) New insights into mechanism and regulation of actin capping protein. *Int Rev Cell Mol Biol* 267: 183–206
45. Russell LD (1979) Further observations on tubulobulbar complexes formed by late spermatids and sertoli cells in the rat testis. *Anat Rec* 194: 213–232
46. Russell LD (1979) Spermatid-sertoli tubulobulbar complexes as devices for elimination of cytoplasm from the head region of late spermatids of the rat. *Anat Rec* 194: 233–246
47. Welch JE, O'Rand MG (1985) Identification and distribution of actin in spermatogenic cells and spermatozoa of the rabbit. *Dev Biol* 109: 411–417
48. Russell LD, Weber JE, Vogl AW (1986) Characterization of filaments within the subacrosomal space of rat spermatids during spermiogenesis. *Tissue Cell* 18: 887–898
49. Geyer CB, Inselman AL, Sunman JA, Bornstein S, Handel MA, Eddy EM (2009) A missense mutation in the Capza3 gene and disruption of F-actin organization in spermatids of repro32 infertile male mice. *Dev Biol* 330: 142–152
50. Dvorakova K, Moore HD, Sebkova N, Palecek J (2005) Cytoskeleton localization in the sperm head prior to fertilization. *Reproduction* 130: 61–69
51. Toyama Y, Iwamoto T, Yajima M, Baba K, Yuasa S (2000) Decapitated and decaudated spermatozoa in man, and pathogenesis based on the ultrastructure. *Int J Androl* 23: 109–115
52. Phelps BM, Koppel DE, Primakoff P, Myles DG (1990) Evidence that proteolysis of the surface is an initial step in the mechanism of formation of sperm cell surface domains. *J Cell Biol* 111: 1839–1847